



HAL
open science

Evaluation of 23 gridded precipitation datasets across West Africa

Frédéric Satgé, Dimitri Defrance, Benjamin Sultan, Marie-Paule Bonnet, F. Seyler, Nathalie Rouche, Fabrice Pierron, Jean-Emmanuel Paturel

► **To cite this version:**

Frédéric Satgé, Dimitri Defrance, Benjamin Sultan, Marie-Paule Bonnet, F. Seyler, et al.. Evaluation of 23 gridded precipitation datasets across West Africa. *Journal of Hydrology*, 2020, 581, 10.1016/j.jhydrol.2019.124412 . hal-02626156v2

HAL Id: hal-02626156

<https://hal.inrae.fr/hal-02626156v2>

Submitted on 23 Nov 2021

HAL is a multi-disciplinary open access archive for the deposit and dissemination of scientific research documents, whether they are published or not. The documents may come from teaching and research institutions in France or abroad, or from public or private research centers.

L'archive ouverte pluridisciplinaire **HAL**, est destinée au dépôt et à la diffusion de documents scientifiques de niveau recherche, publiés ou non, émanant des établissements d'enseignement et de recherche français ou étrangers, des laboratoires publics ou privés.



Distributed under a Creative Commons Attribution 4.0 International License

1 Evaluation of 23 gridded precipitation datasets across West 2 Africa

3 **Frédéric Satgé^{1*}, Dimitri Defrance^{1,2}, Benjamin Sultan¹, Marie-Paule Bonnet¹, Frédérique Seyler¹,**
4 **Nathalie Rouché³, Fabrice Pierron¹, Jean-Emmanuel Paturel³**

5 ¹ESPACE-DEV, Université Montpellier, IRD, Université Guyane, Université Réunion, Université Antilles,
6 Université Avignon, Montpellier, France

7 ²SYSTEM, Université Montpellier, INRA, Montpellier SupAgro, CIRAD, CIHEAM, 34000 Montpellier,
8 France

9 ³HydroSciences Montpellier, IRD, Université de Montpellier, Montpellier, CNRS, Montpellier, France

10 *Corresponding author: frederic.satge@ird.fr

11 Abstract

12 This study aims reporting on 23 gridded precipitation datasets (P-datasets) reliability across West
13 Africa through direct comparisons with rain gauges measurement at the daily and monthly time
14 scales over a 4 years period (2000-2003). All P-datasets reliability vary in space and time. The most
15 efficient P-dataset in term of Kling–Gupta Efficiency (KGE) changes at the local scale and the P-
16 dataset performance is sensitive to seasonal effects. Satellite-based P-datasets performed better
17 during the wet than the dry season whereas the opposite is observed for reanalysis P-datasets. The
18 best overall performance was obtained for MSWEP v.2.2 and CHIRPS v.2 for daily and monthly time-
19 step, respectively. Part of the differences in P-dataset performance at daily and monthly time step
20 comes from the time step used to proceed the gauges adjustment (i.e day or month) and from a
21 mismatch between gauge and satellite reporting times. In comparison to the others P-datasets,
22 TMPA-Adj v.7 reliability is stable and reach the second highest KGE value at both daily and monthly
23 time step. Reanalysis P-datasets (WFDEI, MERRA-2, JRA-55, ERA-Interim) present among the lowest
24 statistical scores at the daily time step, which drastically increased at the monthly time step for
25 WFDEI and MERRA-2. The non-adjusted P-datasets were the less efficient, but, their near-real time
26 availability should be helpful for risk forecast studies (i.e. GSMaP-RT v.6). The results of this study
27 give important elements to select the most adapted P-dataset for specific application across West
28 Africa.

29

30 Keywords: Precipitation datasets, Reliability, West Africa

31 **1. Introduction**

32 **1.1. Precipitation: a key factor subject to uncertainty**

33 Water resources are facing unprecedented changes related to redistribution of seasonal precipitation
34 (Saeed et al., 2018) and intensity (Fischer and Knutti, 2015; Giorgi et al., 2018) owing to climate
35 variability. With a six-fold increase of water extraction during the 20th century in response to
36 increases in the world population (Cosgrove and Risberman, 2000), food requirements and the
37 economy may be particularly affected by these changes. Accurate spatiotemporal precipitation
38 monitoring is therefore crucial for detect and quantifying ongoing changes in optimising water
39 resource management. Traditionally, the precipitation amount is measured at the point scale from
40 gauge measurements. However, access difficulty, political instability, and economic issues have often
41 resulted in sparse and unevenly distributed rain gauge networks that incorrectly capture the spatial
42 precipitation variability (Lebel et al., 1997; Li and D.Heap, 2008). Alternatively, weather radar stations
43 enable precipitation monitoring with spatial distribution over larger and even remote areas.
44 However, radar stations are expensive, and only a few are available worldwide. In addition, large
45 amounts of radar signal interference prevent accurate estimation of precipitation over complex
46 terrains (Tang et al., 2016; Zeng et al., 2018). Several authors have recently reported on the potential
47 of using cellular phone signal attenuation during precipitation events to retrieve precipitation
48 measurements (Doumounia et al., 2014; Messer et al., 2006; Overeem et al., 2011; Zinevich et al.,
49 2008). Although these estimations are accurate, they are limited to regions with high antenna
50 density (e.g. urban areas). Moreover, this technique faces the problem of accessing data owned by
51 private cellular phone companies.

52 Regardless of the technique employed, precipitation data collection at the regional scale usually
53 includes potential conflicts of interest in water resource management between neighbouring
54 countries. In this context, gridded precipitation datasets (P-dataset) at an almost global scale offer an
55 unprecedented alternative. Over remote regions, P-datasets have already shown promising

56 perspective for water resource management by enhancing our understanding of drought (e.g. Agutu
57 et al., 2017; Guo et al., 2017; Satgé et al., 2017; Toté et al., 2015) and flood (e.g. Gao et al., 2017;
58 Nikolopoulos et al., 2013; Toté et al., 2015) events, precipitation variability (e.g. Arvor et al., 2017;
59 Carvalho et al., 2012), streamflow (e.g. Collischonn et al., 2008; De Paiva et al., 2013; Satgé et al.,
60 2019; Sun et al., 2018b; Zhang et al., 2018) and snow cover dynamics (e.g. Satgé et al., 2019), and
61 agriculture productivity (e.g. Thaler et al., 2018; Wit et al., 2010).

62 **1.2. State of the art for P-datasets**

63 Three groups of gridded P-dataset can be defined depending on the input and technique
64 used to retrieve the precipitation amounts: (1) those based on the spatial information of available
65 gauges, (2) those based on reanalysis data derived from physical and dynamical models, and (3)
66 those based on satellite information using passive-microwave (PMW) and infrared (IR) information. It
67 is worth mentioning that most of the P-datasets merge aspects of these three inputs and techniques
68 to ensure the best accuracy possible. Recently, 30 global-scale P-datasets with variable space–time
69 coverage and resolution have been listed (Sun et al., 2018a) which present precipitation estimates
70 discrepancy in space and time according to their different bases such as data capture, integration,
71 and algorithms. For example, gauge-based P-dataset reliability varies in space and time according to
72 changes in the number of available gauges used for the interpolation process (Sun et al., 2015).
73 Similarly, satellite-based P-dataset reliability varies in space and time because the PMW and IR
74 algorithms present limits over complex mountainous (Hussain et al., 2017; Satgé et al., 2017a) and
75 snow-covered regions (Ferraro et al., 1998; Levizzani et al., 2002) and during short-term and slight
76 precipitation events (Gebregiorgis and Hossain, 2013; Tian et al., 2009). Finally, reanalysis data-based
77 P-datasets present variable reliability in space and time owing to the limited ability of the models
78 used to represent small-scale convective cells (Beck et al., 2019). In this context, many studies assess
79 P-dataset space–time uncertainties to evaluate their reliability (Maggioni et al., 2016; Maggioni and
80 Massari, 2018).

81 A recurrent drawback of assessment studies on P-dataset reliability is the consideration of a
82 limited number of P-datasets. A comprehensive reliability overview of available P-datasets, as listed
83 in Table 1, can be achieved only by backcrossing the results from different P-dataset assessment
84 studies. However, the studies are conducted over distinct regions and are based on different
85 statistical indices, spatial and temporal scales, and periods, thus creating difficulties in
86 intercomparing P-dataset reliability assessments. For example, when comparing TMPA, CMORPH,
87 and PERSIANN P-datasets with reference gauge estimates, CMORPH was shown to have the most
88 reliable P-datasets in Pakistan, China, Bali, and Indonesia (Hussain et al., 2017; Rahmawati and
89 Lubczynski, 2017; Su et al., 2017; Zeng et al., 2018). However, TMPA was the most reliable in India,
90 Guyana, Chile, and the South American Andean plateau (Prakash et al., 2014a; Ringard et al., 2015;
91 Satgé et al., 2016; Zambrano-Bigiarini et al., 2017). Hence, P-dataset reliability for a given region
92 should not be determined from results reported for other regions. In this context, it is decisive to
93 consider the most representative P-dataset sample to insure a consistent report on P-dataset
94 reliability across the considered region.

95 **1.3. The need for assessing P-datasets over West Africa**

96 Africa is particularly affected by climate changes threatening rainfed agriculture, which
97 represents its main agricultural and economic activity (Sultan et al., 2013). However, owing to the
98 socio-economic context, the available gauge network is limited by many spatial and temporal gaps
99 which prevent efficient water management. According to the World Meteorological Organisation
100 (WMO), the African continent requires uniform distribution of at least 3000 stations (ideally 10,000);
101 however, only 744 stations are present. Moreover, only one quarter of the 744 stations conform to
102 international standards.

103 Because they provide precipitation information on a regular grid at the global scale, P-
104 datasets offer a unique opportunity for complementing traditional precipitation measurements and
105 optimising population adaption to the ongoing changes. However, as previously mentioned, P-

106 dataset estimates are indirect measurements with spatial and temporal uncertainties which need to
107 be reported to evaluate their reliability. Some authors have already initiated this effort over West
108 Africa. In 2012, seven P-datasets were tested over the basin of la Volta including CMORPH, GPROF-
109 v6, GSMaP-MVK v5, RFE-2.0, TMPA-v6, PERSIANN, and ERA-Interim (Thiemig et al., 2012). In 2013,
110 nine P-datasets including CMORPH, EPSAT-SG, GPCP, GSMaP-MVK, GSMaP-RT, RFE-2, TMPA-v6,
111 TMPA-RT v6, and PERSIANN and seven P-datasets including PERSIANN, CMORPH, TMPA-RT v.6,
112 TMPA-Adj v.6, GSMaP-MVK, GCPC-1dd, and RFE-2 were tested in Benin and Niger for hydrological
113 (Gosset et al., 2013) and agriculture applications (Ramarohetra et al., 2013), respectively. Both
114 studies found that their use could introduce large biases in crop or hydrological modelling
115 framework. More recently, six P-datasets including ARC-2, CMORPH, GSMaP-MVK, PERSIANN,
116 TAMSAT, and TMPA-v.6 were compared with gauge measurements data over the entire African
117 continent (Awange et al., 2016).

118 All of the aforementioned studies focus mainly on P-datasets regularly updated by their
119 developers to enhance the precipitation estimates. Since then, updated versions of the considered
120 products have been made available with more accurate precipitation estimates. For example, the
121 benefits brought by the new TMPA-v.7 in comparison to its previous version (TMPA-v.6) has been
122 reported in many regions (e.g. Anjum et al., 2016; Prakash et al., 2014b; Satgé et al., 2016).
123 Additionally, most of the tested P-datasets originate from the TRMM-era constellation which has
124 limited temporal coverage from 1998 to the present. In this context, new studies have reported on
125 recently released P-dataset versions with larger temporal coverage. For example, in 2016 over
126 Burkina, seven P-datasets including ARC-2, CHIRPS v.2, PERSIANN-CDR, RFE v.2, TAMSAT v.2, TMPA
127 v.7, and TMPA RT v.7 were assessed at the daily, decadal, and monthly timescales (Dembélé and
128 Zwart, 2016). In 2017, TAMSAT v.3 was introduced and compared with its previous version (TAMSAT
129 v.2) and with six P-datasets including ARC v.2, CHIRP v.2, CHIRPS v.2, CMORPH v.1, RFE and TMPA v.7
130 over West Africa, specifically Nigeria and Niger; Uganda; Zambia; and Mozambique (Maidment et al.,
131 2017). In 2017, 10 P-datasets including CFSR, CHIRPS, CMORPH v.1 RAW and CRT, PERSIANN-CDR,

132 RFE-2, TAMSAT v.2, TMPA v.7, TMPA-RT v.7, and GPCC were assessed over six watersheds located in
133 Burkina, Nigeria, and Ghana (Poméon et al., 2017). Nonetheless, the reported studies indicate that
134 the results are mostly limited in space (country or basin scale) and in terms of considered P-datasets
135 sample. To our knowledge, only one study has reported on P-datasets at the regional West African
136 scale with a limited sample of P-datasets including TMPA v.7, UDEL v.3.1, CRU v.3, and ARC v.2
137 (Akinsanola et al., 2016).

138

139 **1.4. Objectives**

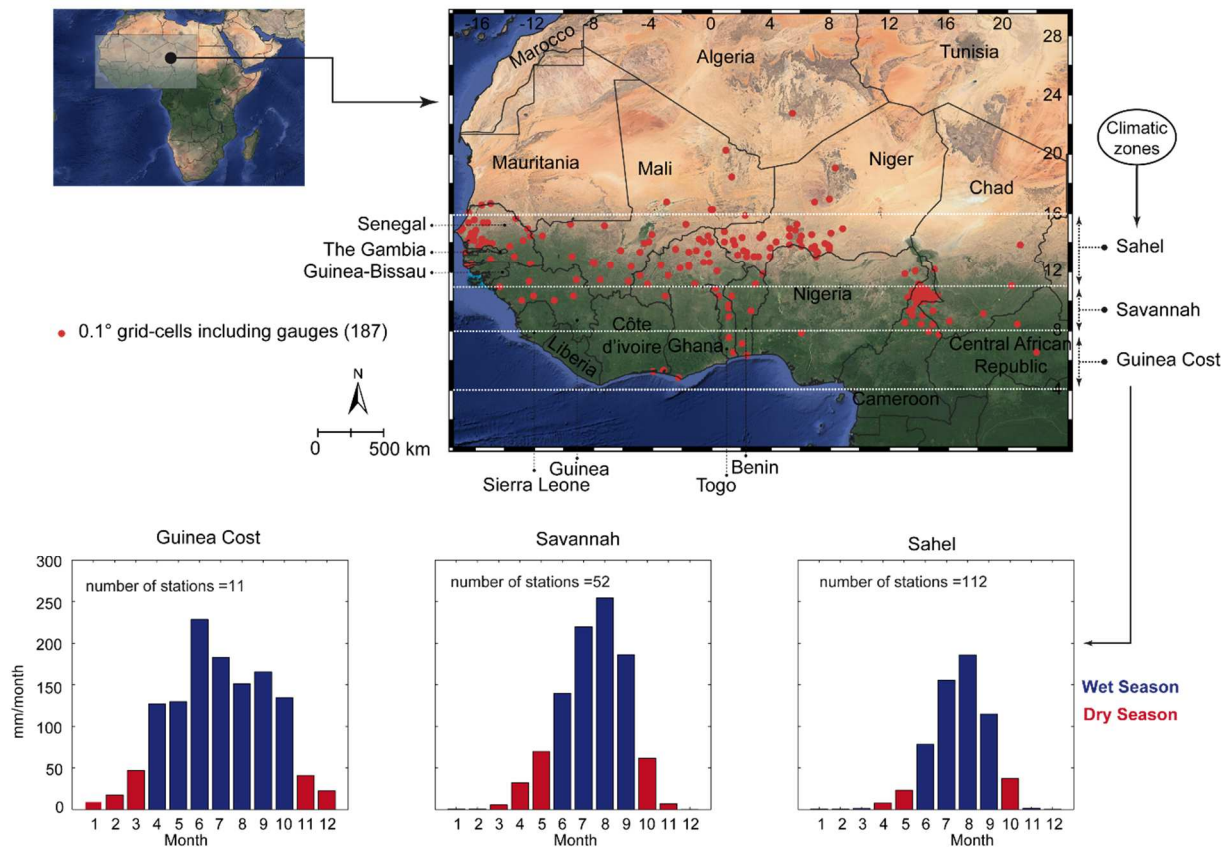
140 According to the previously described context, the present study aims to compare the accuracy of 23
141 P-datasets in reproducing the characteristics of rain gauge measurements across West Africa, which
142 is an unprecedented comparison. The consideration of a P-dataset sample ,as large as possible, aims
143 to provide a robust overview of P-dataset performance over West Africa. The analysis is conducted at
144 both daily and monthly time steps. This study provides important feedback to P-dataset developers
145 for enhancing the algorithms for next-generation P-datasets and to potential users to support their
146 P-datasets selection.

147 **2. Materials Methods**

148 **2.1. Study Area**

149 The study area, hereafter referred to as West Africa, extends from the Atlantic coast of Senegal to
150 eastern Chad and the Gulf of Guinea to north of the Sahel (18° W–25° E, 4° N–25° N) (Fig. 1). The
151 region is characterised by a marked south–north gradient of rainfall amount ranging from 5000
152 mm.year⁻¹ in Cameroon to less than 200 mm.year⁻¹ in the northern Sahel. The West Africa region can
153 be divided into three main climatic zones: (i) the Guinea Coast (4°–8° N), (ii) the Savannah (8°–11° N),
154 and (iii) the Sahel (11°–16° N) (Abiodun et al., 2012; Akinsanola et al., 2016) (Fig. 1). For all zones, the
155 year is characterised by a dry season in winter and a rainy season in summer linked to the West
156 African Monsoon. This concentrates most of the annual rainfall amount from April to October for the

157 Guinea Coast zone and from June to September for both the Savannah and Sahel zones (Fig. 1). The
 158 rainfall interannual temporality is great with the occurrence of drought phases (dry spell) during the
 159 rainy season and in interannual rainfall with very dry and very wet years in the 1970s and 1950s,
 160 respectively.



161
 162 *Figure 1. Study area with the considered 0.1° grid-cell locations and the mean monthly precipitation amount given for the*
 163 *three climatic regions based on gauge records of 2000–2003.*

164 **2.2. Selected P-datasets**

165 A sample of 23 gridded P-datasets including 13 long-term P-datasets with more than 35 years of
 166 continuous observation and 10 P-datasets spanning more than 15 years was selected. Table 1
 167 provides an overview of these P-datasets and relevant references for further information on their
 168 respective productions.

169

Acronym	Full Name	Data	Temporal Coverage	Temporal Resolution	Spatial Coverage	Spatial Resolution	Latency	Link	References
ARC-2	Africa Rainfall Climatology v.2	S, G	1983–present	Daily	Africa	0.1°	2 days	ftp://ftp.cpc.ncep.noaa.gov/fews/fewsdata/africa/arc2/	Novella and Thiaw, 2012
CHIRP v.2	Climate Hazards Group InfraRed v.2	S, R	1981–present	Daily	50°	0.05°	2 days	ftp://ftp.chg.ucsb.edu/pub/org/chg/products/	Funk et al. (2015)
CHIRPS v.2	CHIRP with Station v.2	S, R, G	1981–present	Daily	50°	0.05°	1 month	ftp://ftp.chg.ucsb.edu/pub/org/chg/products/	Funk et al. (2015)
CMORPH-Raw v.1	Climate Prediction Center MORPHing raw v.1	S	1998–present	3 h	60°	0.25°	2 days	ftp://ftp.cpc.ncep.noaa.gov/precip/CMORPH_V1.0/	Joyce et al. (2004)
CMORPH-CRT v.1	CMORPH bias corrected v.1	S, G	1998–present	3 h	60°	0.25°	6 months	ftp://ftp.cpc.ncep.noaa.gov/precip/CMORPH_V1.0/	Xie et al. (2017)
CMORPH-BLD v.1	CMORPH satellite-gauge merged v.1	S, G	1998–present	Daily	60°	0.25°	10 months	ftp://ftp.cpc.ncep.noaa.gov/precip/CMORPH_V1.0/	Xie et al. (2017)
CPC v.1	Climate Prediction Center unified v.1	G	1979–present	Daily	Global	0.5°	1 days	ftp://ftp.cpc.ncep.noaa.gov/precip/CPC_UNI_PRCP/GAUGE_GLB/	Xie et al. (2007) Chen et al. (2008)
ERA-Interim	European Centre for Medium-range Weather Forecast Re Analysis Interim	R	1979–present	3 h	60°	0.75°	3 months	https://www.ecmwf.int/en/forecasts/datasets/reanalysis-datasets/era-interim-land	Dee et al. (2011)
GSMaP-RT v.6	Global Satellite Mapping of Precipitation standard v.6	S	2000–present	Hourly	60°	0.1°	3 days	ftp://hokusai.eorc.jaxa.jp/standard/v6/	Ushio et al. (2009) Yamamoto and Shige (2014)
GSMaP-Adj v.6	GSMaP adjusted v.6	S, G	2000–resent	Hourly	60°	0.1°	3 days	ftp://hokusai.eorc.jaxa.jp/standard/v6/	Ushio et al. (2009) Yamamoto and Shige (2014)
GPCC v.7	Global Precipitation Climatology Center	G	1901–2013	Monthly	Global	1°	Irregular	https://rda.ucar.edu/datasets/ds496.0/	Becker et al., 2013; Schneider et al., 2014
JRA-55	Japanese 55-year Re Analysis	R	1959–present	3 h	Global	0.56°	1 Month	https://rda.ucar.edu/datasets/ds628.0/	Kobayashi et al. (2015)
JRA-55 Adj	JRA-55 Adjusted	R, G	1959–2013	3 h	Global	0.56°	Stopped	http://search.diasjp.net/en/dataset/S14FD	Izumi et al. (2017)
MERRA-2	Modern-Era Retrospective Analysis for Research and Applications 2	S, R, G	1980–present	Hourly	Global	0.5°	2 Months	https://disc.gsfc.nasa.gov/	Gelaro et al. (2017) Reichle et al. (2017)
MSWEP v.2.2	Multi-Source Weighted Ensemble Precipitation v.2.2	S, R, G	1979–present	3h	Global	0.1°	Few months	http://www.gloh2o.org/ (Personal communication)	Beck et al. (2018) Beck et al. (2019)
PERSIANN-CDR	Precipitation Estimates from Remotely Sensed Information using Artificial Neural Network and Climate Data Record	S, G	1983–2016	Daily	60°	0.25°	6 months	https://chrsdata.eng.uci.edu/	Ashouri et al. (2015)
PERSIANN-RT	PERSIANN real time	S	2000–present	6 h	60°	0.25°	2 days	https://chrsdata.eng.uci.edu/	Hsu et al. (1997) Sorooshian et al. (2000)
PERSIANN-Adj	PERSIANN Adjusted	S, G	2000–2010	3 h	60°	0.25°	Stopped	http://fire.eng.uci.edu/PERSIANN/	Hsu et al. (1997) Sorooshian et al. (2000)
SM2Rain-CCI v.2	Soil Moisture to Rain applied on ESA Climate Change Initiative v.2	S	1998–2015	Daily	Global	0.25°	Stopped	https://zenodo.org/record/846260#.XQZtYgzZaQ	Ciabatta et al. (2018)

<i>TAMSAT-v.3</i>	Tropical Applications of Meteorology using SATellite and ground-based observations v.3	S, G	1983–present	Daily	Africa	0.0375°	3 days	https://www.tamsat.org.uk/about	Maidment et al. (2017)
<i>TMPA-RT v.7</i>	TRMM Multi-satellite Precipitation Analysis Real Time v.7	S	1998–present	3 h	60°	0.25°	1 day	https://mirador.gsfc.nasa.gov/	Huffman et al. (2018) Huffman et al. (2010)
<i>TMPA-Adj v.7</i>	TMPA Adjusted v.7	S, G	2000–present	3 h	50°	0.25°	3 months	https://earthdata.nasa.gov/	Huffman et al. (2018) Huffman et al. (2010)
<i>WFDEI</i>	WATCH Forcing Data methodology applied to ERA-Interim	R, G	1979–2016	Daily	Land	0.5°	Stopped	ftp://ftp.iiasa.ac.at/	Weedon et al. (2014)

170

171 *Table 1. Main characteristics and references of the P-datasets. In the data source column, S, R, and G stands for satellite,*
172 *reanalysis, and gauge information. Spatial coverage refers to the absolute maximum and minimum latitude with*
173 *precipitation information, and latency refers to the time delay for data availability. The P-datasets including gauge-based*
174 *information are represented in blue, and italic font is used for P-datasets available in NRT latency of one to three days.*

175 **2.2.1. Comments on the selected P-datasets**

176 Some P-datasets use gauge-based information in their respective algorithms (Table 1). Three types of
177 gauge-based information are used: (1) punctual precipitation estimates derived from gauge records,
178 (2) gridded precipitation estimates based on interpolation of punctual gauge records, and (3) gauge
179 precipitation estimates (punctual or gridded) merged with different satellite datasets of
180 precipitation, brightness, or land surface temperature.

181 Punctual precipitation estimates from the world meteorological organisation (WMO) Global
182 Telecommunication System (GTS) (Novella and Thiaw, 2012) and numerous African national
183 meteorological and hydrological centres (Maidment et al., 2014) are used for ARC-2 and TAMSAT v.3,
184 respectively. In both cases, the gauge network is very sparse. For example, the GTS gauge network
185 has a 1:23 000 km² gauge-to-area ratio across the African continent (Novella and Thiaw, 2012).

186 The gridded precipitation estimates are (i) GPCC with a 1° spatial resolution (Becker et al.,
187 2013; Schneider et al., 2014) and (ii) the daily CPC with 0.5° spatial resolution (Chen et al., 2008; Xie

188 et al., 2007). JRA-55 Adj, TMPA-Adj v.7, and WFDEI use GPCP monthly data, whereas CMORPH-CRT
189 v.1, CMORPH-BLD v.1, GSMaP-Adj v.6, and MERRA-2 use CPC daily data.

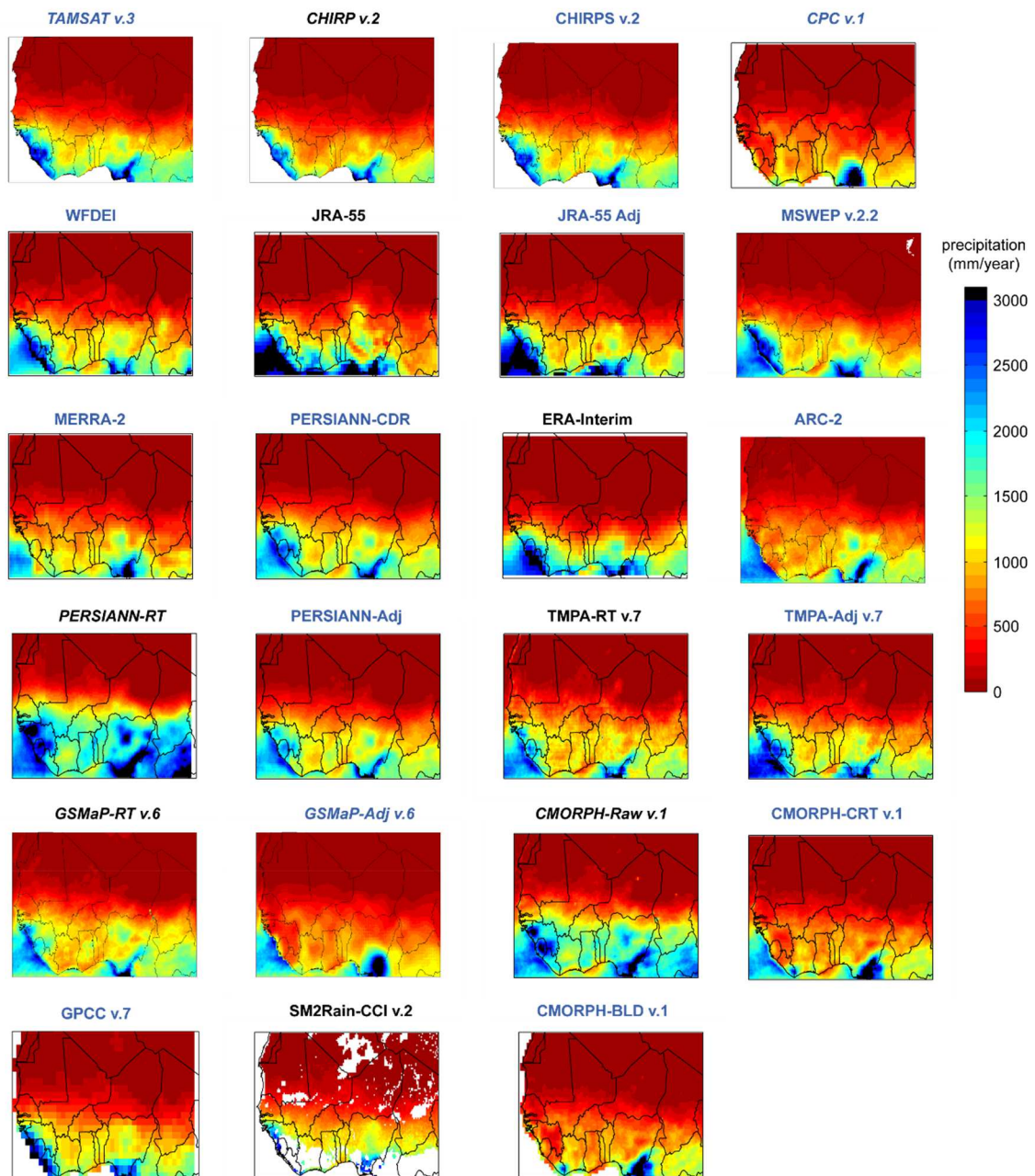
190 The gridded precipitation estimates merged with satellite precipitation estimates are (i) the
191 CHPclim dataset with a 0.05° grid-cell size (Funk et al., 2015) and (ii) the GPCP dataset with a 2.5°
192 grid-cell size (Adler et al., 2003, 2012) and (iii) the WorldClim 2 dataset with a 1km grid-cell size (Fick
193 and Hijmans, 2017). CHPclim and WorldClim 2 use satellite observations as predictors to improve the
194 interpolation from point gauge records, whereas GPCP uses the gauge record to adjust the
195 precipitation fields derived from satellite observations. Further details are reported elsewhere (Adler
196 et al., 2003; Funk et al., 2015). Among the considered P-datasets, CHIRPS v.2 use the CHPclim
197 dataset, MSWEP v.2.2 use the WorldClim 2 dataset and PERSIANN-CDR uses the GPCP dataset.

198 CHIRPS v.2 also includes punctual precipitation estimates from various public data streams,
199 private archives, and national meteorological agencies, while MSWEP v.2.2 incorporates monthly
200 GPCP and daily CPC gridded precipitation datasets.

201 Another difference between the P-datasets is the time latency for their availability. The P-
202 datasets are generally available in (i) a few days or (ii) a few months after the observation (Table 1).
203 Some are in near real time (NRT) latency of one to three days and are more adapted for flood or
204 landslides forecasting, water resource management, and agriculture, while the others are more
205 adapted for retrospective climatic studies.

206 Figure 2 shows the mean annual precipitation patterns retrieved from all P-datasets. Except for
207 CPC v.1 and the P-datasets, which use CPC v.1 for post adjustment processing (ARC-2, CMORPH-CRT
208 v.1, CMORPH-BLD v.1, GSMaP-Adj v.6 and MERRA-2), all P-datasets represent the typical south–north
209 precipitation gradient with two precipitation hotspots located over the southwest and south region.
210 It should be noted that SM2Rain-CCI v.2 estimates are based on soil moisture estimates, which are
211 strongly attenuated by the vegetation canopy; this results in significant gaps over areas with
212 moderate to dense vegetation, as observed over the southern region (Fig. 2) (Dorigo et al., 2015).

213 Additionally, a sensor failure in the ERS-2 gyroscope from January 2001 to June 2003 accentuated
 214 these gaps and explains the gaps observed over the central and northern regions (Fig. 2) (Dorigo et
 215 al., 2015).



216
 217 *Figure 2. Mean annual precipitation for 2000–2003 retrieved from all P-datasets at their original grid sizes. For each P-*
 218 *dataset, only the grid-cells with more than 80% of available daily data were retained. Blue and black colours are used to*
 219 *highlight P-datasets using and not using gauge-based information, respectively, and italic font is used for P-datasets*
 220 *available in NRT latency of one–three days.*

221 **2.2.2. P-dataset pre-processing**

222 The P-datasets available at a sub-daily time step (Table 1) were aggregated to obtain daily time step
223 records matching the local gauge observations (8 h to 8 h local time). It is worth mentioning that P-
224 datasets delivered at daily time scales (Table 1) use time-windows different from those of the gauge,
225 which can compromise the comparison at the daily scale. This point is further discussed in section
226 4.1. Moreover, the P-datasets differ in terms of grid-cell size, ranging from 0.0375° for TAMSAT v.3 to
227 1° for GPCC v.7. To enable consistent comparison, all P-datasets were resampled to the 0.1° grid-cell
228 size.

229 Bilinear averaging (interpolation) are used for P-datasets with grid-cell size < 0.1° (> 0.1°) (Beck et al.,
230 2019).

231 **2.3. Reference precipitation dataset**

232 A database of 1,440 gauges were made available by several African national meteorological and
233 hydrological centres. The stations are distributed onto 952 0.1° grid-cells. For each grid-cell, a
234 reference daily precipitation series was obtained averaging the gauges included in the grid-cell. To
235 ensure consistent analysis, only grid-cells with more than 80% of daily records were considered. The
236 four-year period of 2000–2003 was finally retained to consider the largest number of 0.1° grid-cells
237 (187) grid-cells.

238 **2.4. Monthly P-dataset estimate assessment**

239 The monthly amounts were computed for only months with more than 80% of common daily records
240 for all datasets (reference and P-datasets). The accuracy of monthly P-dataset estimates was
241 assessed using a quantitative statistical analysis based on the modified Kling–Gupta Efficiency (KGE),
242 an objective function combining correlation (r), bias (β), and variability (γ) components (Gupta et
243 al., 2009; Kling et al., 2012) (Eq. 1). We used KGE because water resource management requires
244 reliable representation of precipitation temporal dynamics (measured by r) and volume (measured
245 by β and γ):

$$KGE = 1 - \sqrt{(r - 1)^2 + (\beta - 1)^2 + (\gamma - 1)^2}, \quad (1)$$

246 where r represents the Pearson coefficient (Eq. 2), β is the ratio between the mean observed and
 247 predicted precipitation (Eq. 2), and γ is the ratio of the estimated and observed coefficients of
 248 variation (eq. 3):

249

$$r = \frac{1}{n} \sum_{i=1}^n \frac{(o_n - \mu_o) * (s_n - \mu_s)}{\sigma_o * \sigma_s}, \quad (2)$$

$$\beta = \frac{\mu_s}{\mu_o}, \quad (3)$$

$$\gamma = \frac{\sigma_s/\mu_s}{\sigma_o/\mu_o}, \quad (4)$$

250 where μ and σ are the distribution mean and standard deviation, respectively; and s and o indicate
 251 the estimate and reference, respectively. KGE , β , γ , and r have their optimum at unity.

252 The analysis was performed considering all months of 2000–2003 and the wet and dry seasons
 253 months separately. For each grid-cell, the wet and dry seasons were selected according to their
 254 corresponding climatic zone (Fig. 1). The Sahel seasonality was applied for the grid-cells located up to
 255 latitude 16° N.

256 The values of KGE , r , β , and γ were computed at each grid-cell location to observe the P-dataset
 257 reliability over space, and their median values was used to observe that at the regional scale.

258 Considering the important gaps over space and time for SM2Rain-CCI v.2 (Fig. 2), its performance
 259 analysis was based on a reduced number of 0.1° grid-cells (79). Finally, GPCC v.7 is only available at
 260 the monthly time step (table 1). Consistent comparison between GPCC v.7 and the reference was
 261 possible only for grid-cells and months with complete daily observation series for a total of 183 grid-
 262 cells.

263 **2.5. Daily P-dataset estimate assessment**

264 The daily precipitation estimates were assessed on the basis of on both quantitative and categorical
 265 statistical metrics. The quantitative analysis relied on the median KGE, r , β , and γ obtained from the
 266 187 considered grid-cells for all days and the wet and dry seasons days, separately, and from the
 267 79 (183) grid-cells for SM2Rain-CCI v.2 (GPCC v.7).

268 The categorical statistics were used to measure the P-dataset capacity for detecting the daily
 269 precipitation events. Daily precipitation events are considered as discrete values with only two
 270 observable cases: rainy or not rainy days. A rainy day was considered when the precipitation amount
 271 was greater than or equal to a prescribed threshold (mm.day^{-1}). Four cases were possible (Table 2).
 272 Based on this characterisation, the Heidke Skill Score (HSS) (Eq. 4) evaluates the P-dataset ability for
 273 detecting precipitation events in comparison with a random based prediction.

274 *Table 2. Contingency table used to define HSS*

		Rain gauges	
		Precipitation	No precipitation
P-datasets	Precipitation	a	b
	No precipitation	c	d

275

276

$$HSS = \frac{2 * (a * d - b * c)}{[(a + c) * (c + d) + (a + b) * (b + d)]} \quad (5)$$

277

278 The HSS values range from $-\infty$ to 1 with a perfect score of 1 and negative values indicating
 279 that random based prediction outperforms the P-dataset one.

280 The mean HSS value was computed from those obtained for all of the considered grid-cells for
 281 threshold values ranging from 0 to 25 mm.day^{-1} with a 1 mm.day^{-1} increment. This consideration was
 282 used to assess the P-dataset performance based on light to heavy daily precipitation events. Finally,

283 using a $1\text{mm}\cdot\text{day}^{-1}$, the HSS value was computed at each grid-cell location to observe the P-dataset
284 reliability over space.

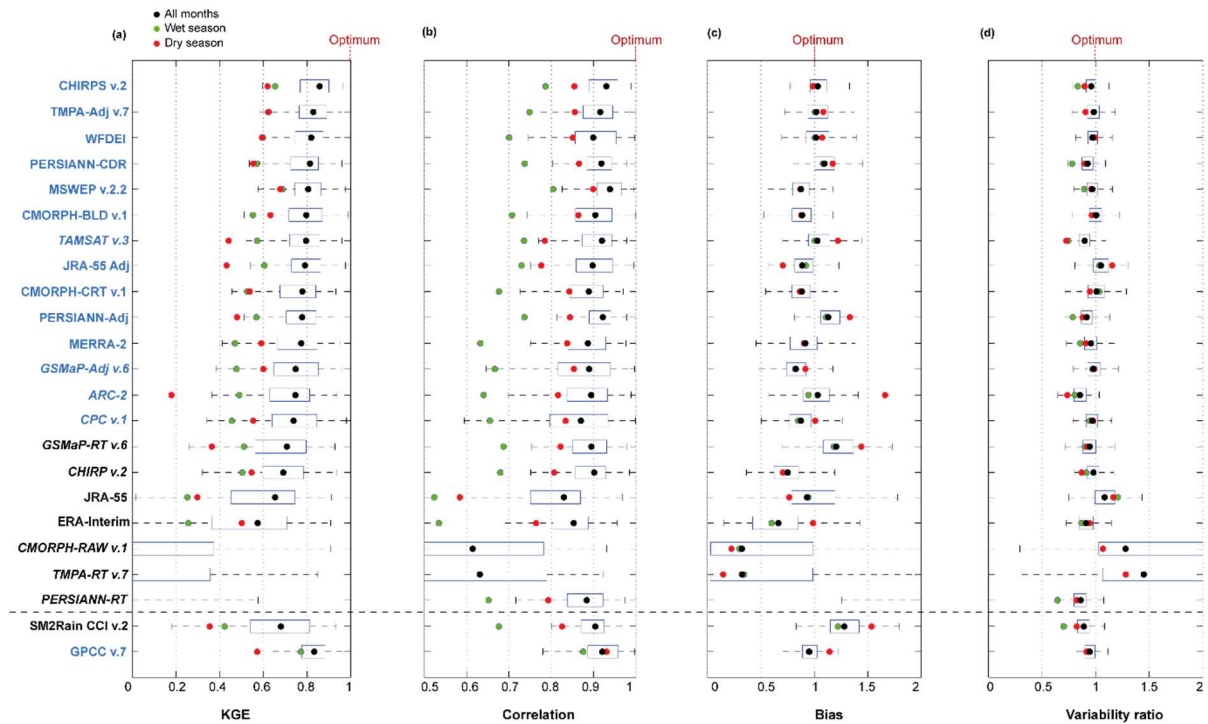
285

286 **3. Results**

287 **3.1. P-dataset assessment at the monthly time step**

288 With negative KGE values, three P-datasets (CMORPH-Raw v.1, TMPA-RT v.7, and PERSIANN-RT),
289 were unable to represent the regional monthly precipitation (Fig.3). Interestingly, their adjusted
290 versions, CMORPH-BLD v.1, TMPA-Adj v.7, and PERSIANN-CDR, respectively, performed much better
291 with KGE greater than 0.8, correlation better than 0.9, and bias and variability close to the optimum
292 values (1). The same results were shown for CHIRP v.2, GSMaP-RT v.6, and JRA-55, which were
293 systematically outperformed by their corresponding adjusted versions (CHIRPS v.2, GSMaP-Adj v.6,
294 and JRA-55 Adj, respectively). In a general way, all P-datasets using gauges-based information
295 present higher KGE than the others. The P-datasets developed for the African continent, TAMSAT v.3
296 and ARC-2, did not outperform the global scale P-datasets. However, the TAMSAT v.3 reliability was
297 very close to that of the other P-datasets (KGE = 0.8).

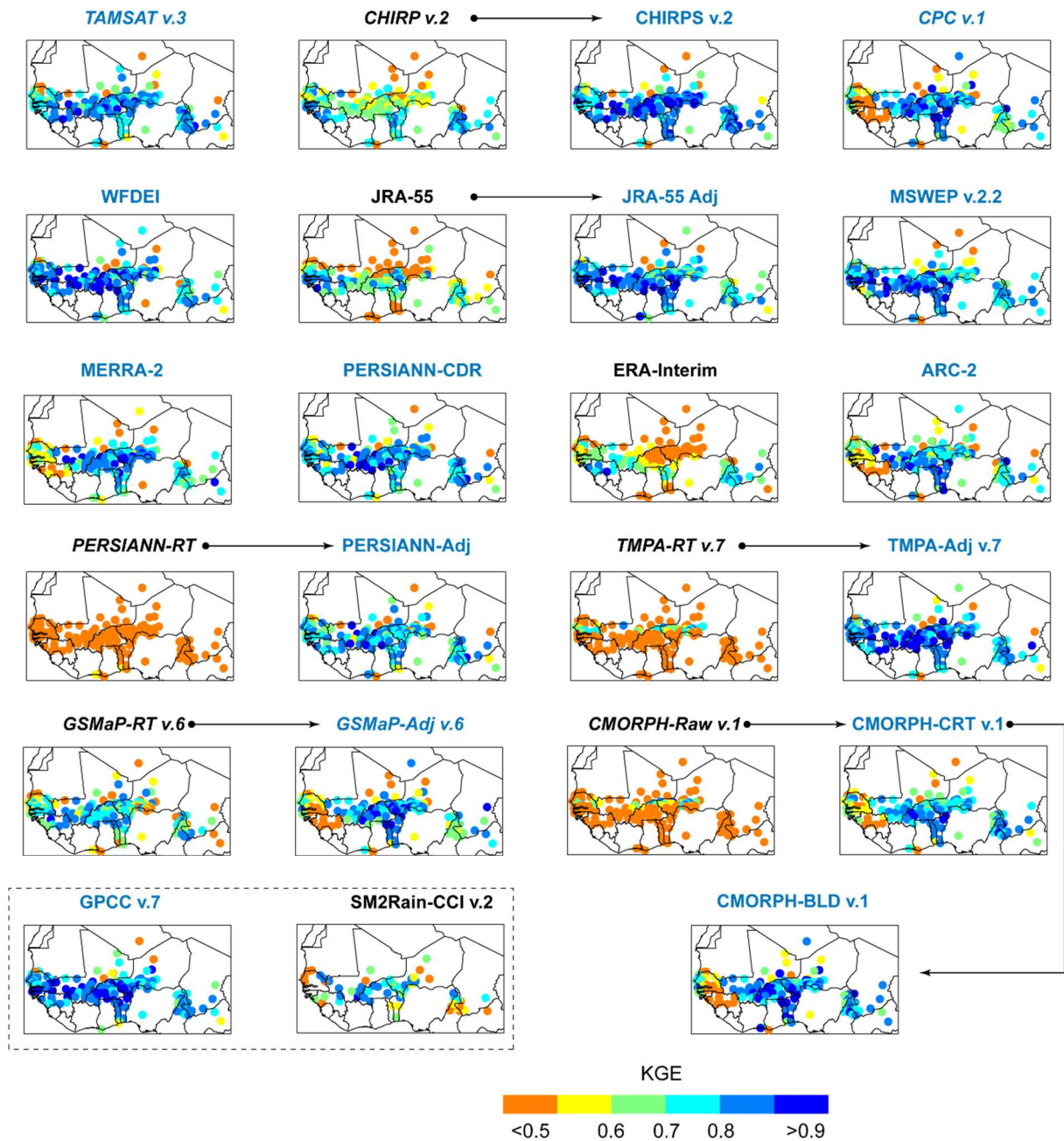
298 The P-dataset performance expressed as KGE varied seasonally. P-datasets TAMSAT v.3, JRA-
299 55 Adj, PERSIANN-Adj, ARC-2, GSMaP-RT v.6, and GPCC v.7 were more effective during the wet
300 season, and CMORPH-BLD v.1, MERRA-2, GSMaP-Adj v.6, CPC v.1, and ERA-Interim had better
301 performance during the dry season. However, the most effective P-datasets, CHIRPS v.2, TMPA-Adj
302 v.7, WFDEI, PERSIANN-CDR, and MSWEP v.2.2, performed similarly for both wet and dry seasons.
303 Interestingly, all P-datasets presented higher correlation coefficient and bias values during the dry
304 season. With respect to the variability ratio, no clear seasonal trend was observed for the different P-
305 datasets.



306

307 *Figure 3. P-dataset reliability at the regional. The right and left edges of the boxes represent the 25th and 75th percentile*
 308 *values, respectively. The P-datasets are sorted from the most (top) to the least (bottom) efficient in term of KGE. SM2Rain-*
 309 *CCI v.2 and GPCCC v.7 are at the bottom because their analyses are based on a different number of 0.1° grid-cells, at 79 and*
 310 *183, respectively. Blue and black colours are used to highlight P-datasets using or not using gauge-based information,*
 311 *respectively, and italic font is used for P-datasets available in NRT latency of one to three days. The graphics were inspired*
 312 *by Beck et al. (2019).*

313 Adjustment of CHIRP v.2, JRA-55, PERSIANN-RT, TMPA-RT v.7, GSMaP-RT v.6, and CMORPH-
 314 Raw v.1 increased the KGE values considerably at most of the grid-cell locations. The adjustment
 315 applied to GSMaP-Adj v.6 was not effective over the western region, where KGE values decreased in
 316 comparison to GSMaP-RT v.6, its non-adjusted version. Similarly, the CMORPH adjusted versions
 317 (CMORPH-CRT v.1 and BLD v.1) presented the lowest registered KGE values over the western region.
 318 CPC v.1, MERRA-2, and ARC-2 also presented the lowest KGE value over this region. Regarding the
 319 most effective P-datasets, CHIRPS v.2, GPCCC v.7, WFDEI, and TMPA-Adj v.7 presented similar KGE
 320 distributions.



321

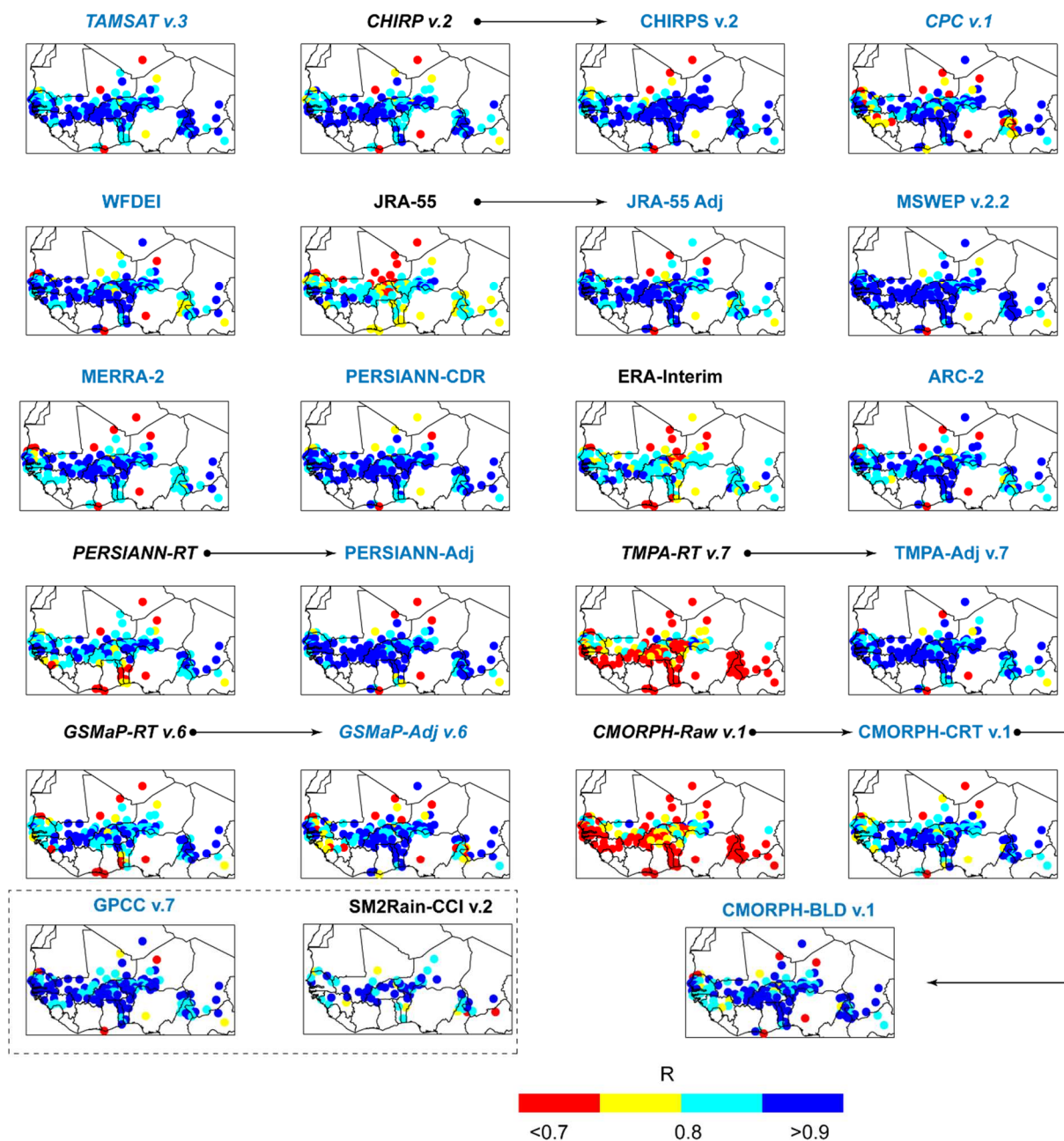
322 *Figure 4. P-dataset reliability at the grid-cell level expressed in the form of KGE considering all months in 2000–2003. Arrows*
 323 *are used to highlight the potential benefit of using gauge-based information. Blue and black colours are used to highlight P-*
 324 *datasets using or not using gauge-based information, respectively, and italic font is used for P-datasets available in NRT*
 325 *latency of one the three days.*

326 Most of the P-datasets were well correlated to the reference, with correlation better than 0.8 (Fig.5).

327 The adjusted version systematically presented higher correlation values, with MSWEP v.2.2

328 presenting the highest number of grid-cells with correlation better than 0.9 and only one grid-cell

329 with correlation worse than 0.7. Interestingly, CHIRPS presented the lowest correlation score over
 330 the northern very arid region, with correlation worse than 0.7 (Fig.5).

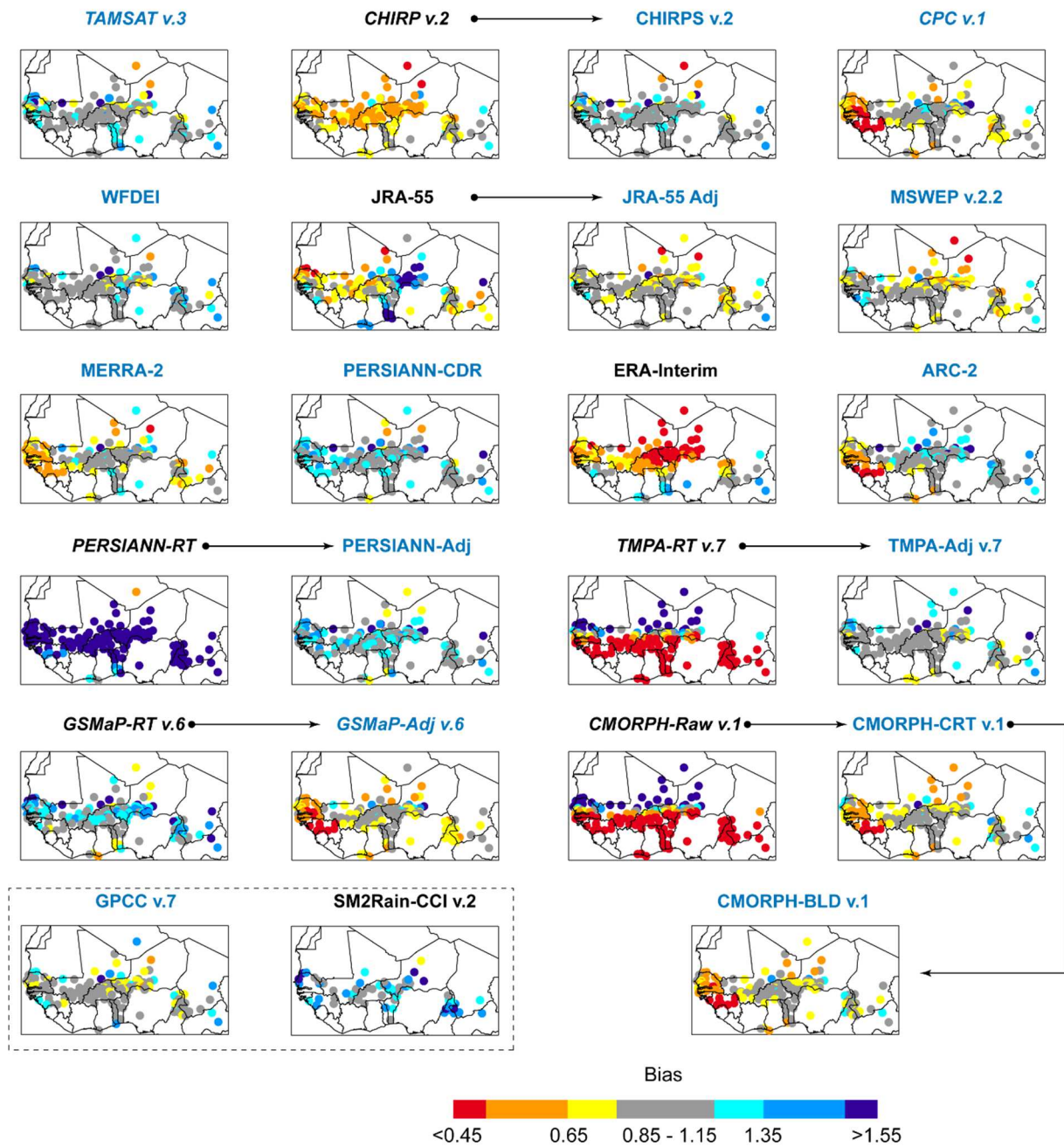


331
 332 *Figure 5. P-dataset reliability at the grid-cell scale expressed in the form of correlation considering all months in 2000–2003.*
 333 *Arrows are used to highlight the potential benefit of using gauge-based information. Blue and black colours are used to*
 334 *highlight P-datasets using or not using gauge-based information, respectively, and italic font is used for P-datasets available*
 335 *in NRT latency of one to three days.*

336 The P-datasets without gauge-based information presented higher bias (Fig.6). PERSIANN-RT highly
337 overestimate precipitation throughout the region (bias > 1.55). The bias decreased in the post-
338 adjusted version (PERSIANN-Adj) with acceptable bias estimates ($1.15 < \text{bias} < 1.35$) over many grid-
339 cells

340 Similar results were observed for PERSIANN-CDR. CMORPH-Raw v.1 and TMPA-RT v.7 presented
341 similar bias distributions, from overestimation to underestimation in the northern arid and southern
342 humid regions, respectively. TMPA-RT gauge adjustment was highly successful, with most of the
343 TMPA-Adj v.7 grid-cells presenting acceptable bias values at $0.85 < \text{bias} < 1.15$. CPC v.1 strongly
344 underestimates precipitation over the western region. This bias spread for all P-datasets using CPC
345 v.1 for their adjustment process (CMORPH-CRT and BLD v.1, ARC-2, GSMaP-Adj v.6 and MERRA-2).

346 Interestingly, the precipitation adjustment applied on GSMaP-RT v.6 increased the bias on GSMaP-
347 Adj v.6. WFDEI, TMPA-Adj v.7, and CHIRPS v.2 presented less-biased precipitation estimates with
348 reasonable bias values of $0.85 < \text{bias} < 1.15$ in most of the considered grid-cells.



349

350 *Figure 6. P-dataset reliability at the grid-cell scale expressed in the form of bias considering all months for in 2000–2003.*

351 *Arrows are used to highlight the potential benefit of using gauge-based information. Blue and black colours are used to*

352 *highlight P-datasets using or not using gauge-based information, respectively, and italic font is used for P-datasets available*

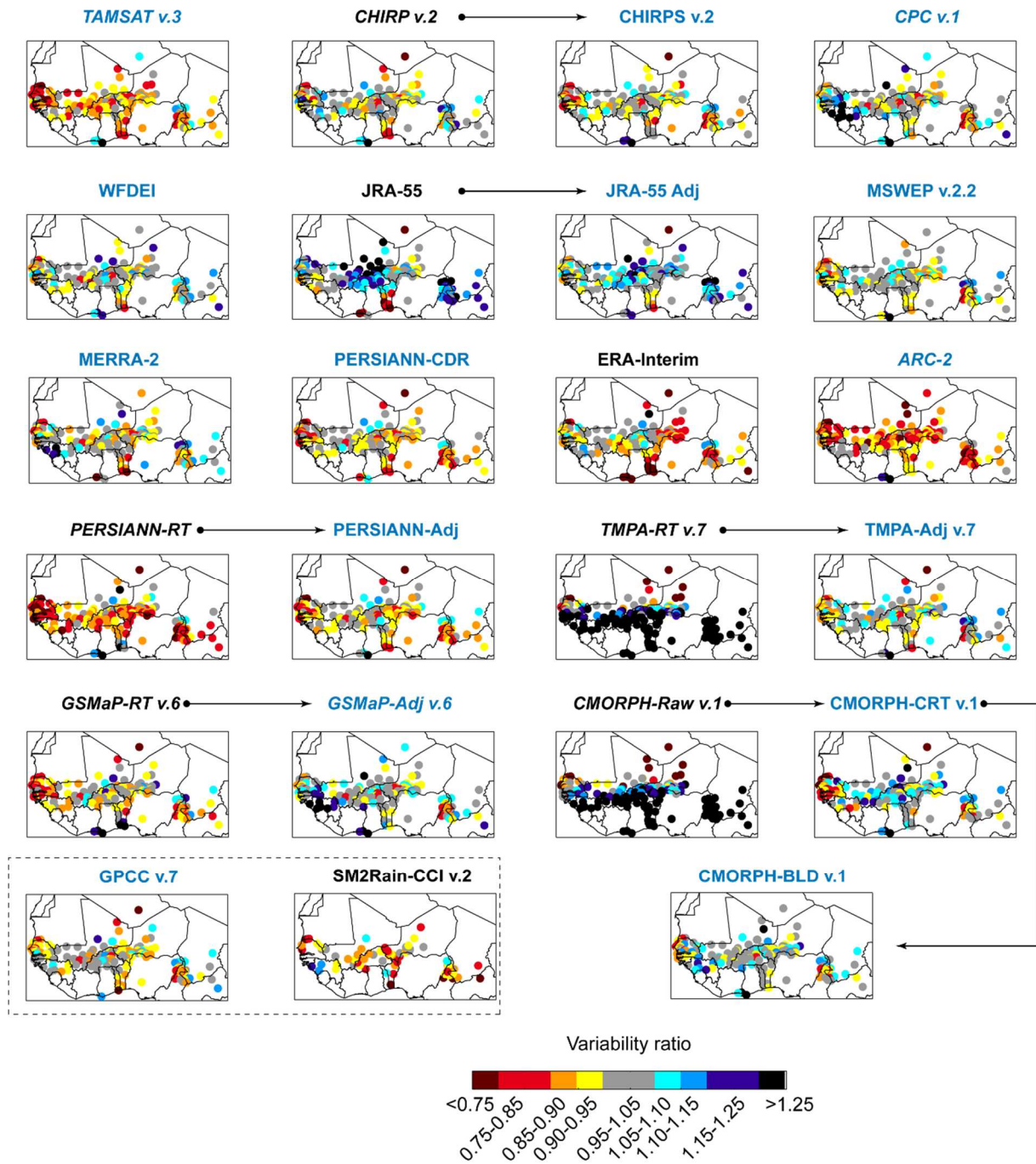
353 *in NRT latency of one to three days.*

354 Regarding the variability ratio distribution, the efficiency of using gauge-based information to

355 retrieve the precipitation estimates was obvious when comparing PERSIANN-RT, TMPA-RT v.7, and

356 CMORPH-Raw v.1 with their post-adjusted versions (Fig.7). The non-adjusted products CMORPH-

357 RAW v.1, and TMPA-RT v.7 strongly overestimated the precipitation variability in the majority of grid-
358 cells with variability ratios better than 1.25. To the contrary, PERSIANN-RT strongly underestimated
359 the precipitation variability in most grid-cells, with a variability ratio worse than 0.85. However, when
360 considering JRA-55 (JRA-55 Adj) and CHIRP v.2 (CHIRPS v.2), the use of gauge-based information did
361 not significantly enhance the variability ratio. Finally, the two African P-datasets underestimated the
362 precipitation variability, over most of the grid-cells (variability ratios < 0.90).



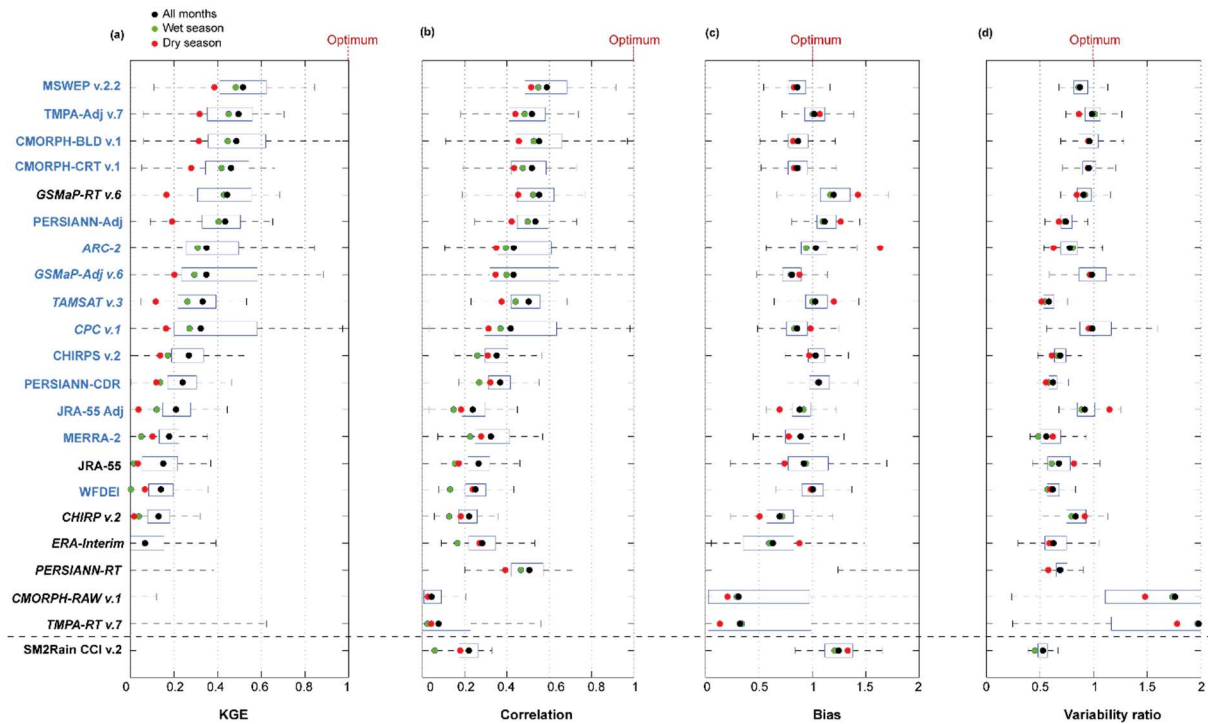
363

364 *Figure 7. P-dataset reliability at the grid-cell scale expressed in the form of variability ratio considering all months for in*
 365 *2000–2003. Arrows are used to highlight the potential benefit of using gauge-based information. Blue and black colours are*
 366 *used to highlight P-datasets using or not using gauge-based information, respectively, and italic font is used for P-datasets*
 367 *available in NRT latency of one to three days.*

368 3.2. P-dataset assessment at the daily time step

369 At the regional scale, the ability of the P-datasets to quantify the daily precipitation amount was
370 relatively low, with most having median KGE values worse than 0.4 (Fig.8). Only MSWEP v.2.2, TMPA-
371 Adj v7, CMORPH-BLD v.1, CMORPH-CRT v.1, GSMaP-RT v.6, and PERSIANN-Adj had KGE scores
372 superior to 0.4, with the best score achieved by MSWEP v.2.2 (KGE = 0.52). Generally, non-adjusted
373 P-datasets presented the lowest KGE values except for GSMaP v.6. The KGE decreased from 0.44
374 (GSMaP-RT v.6) to 0.35 for (GSMaP-Adj v.6). Interestingly, PERSIANN-RT presented a negative KGE
375 value but one of the highest correlation score, at 0.5. Therefore, its low KGE score appears to be
376 influenced by its very high positive bias value of 2.5. This is in line with observation made at the
377 monthly time step and the dominant influence of the bias values on the KGE score.

378 In term of KGE, the P-dataset accuracy was higher during the wet than that in the dry season.
379 Interestingly, MERRA-2, WFDEI, ERA-Interim, and JRA-55 performed better during the dry season,
380 which is line with the results obtained over the Continental United States (CONUS) (Beck et al., 2019).
381 However, the performances of MERRA-2, WFDEI, ERA-Interim, and JRA-55 were very low, with KGE <
382 0.2.

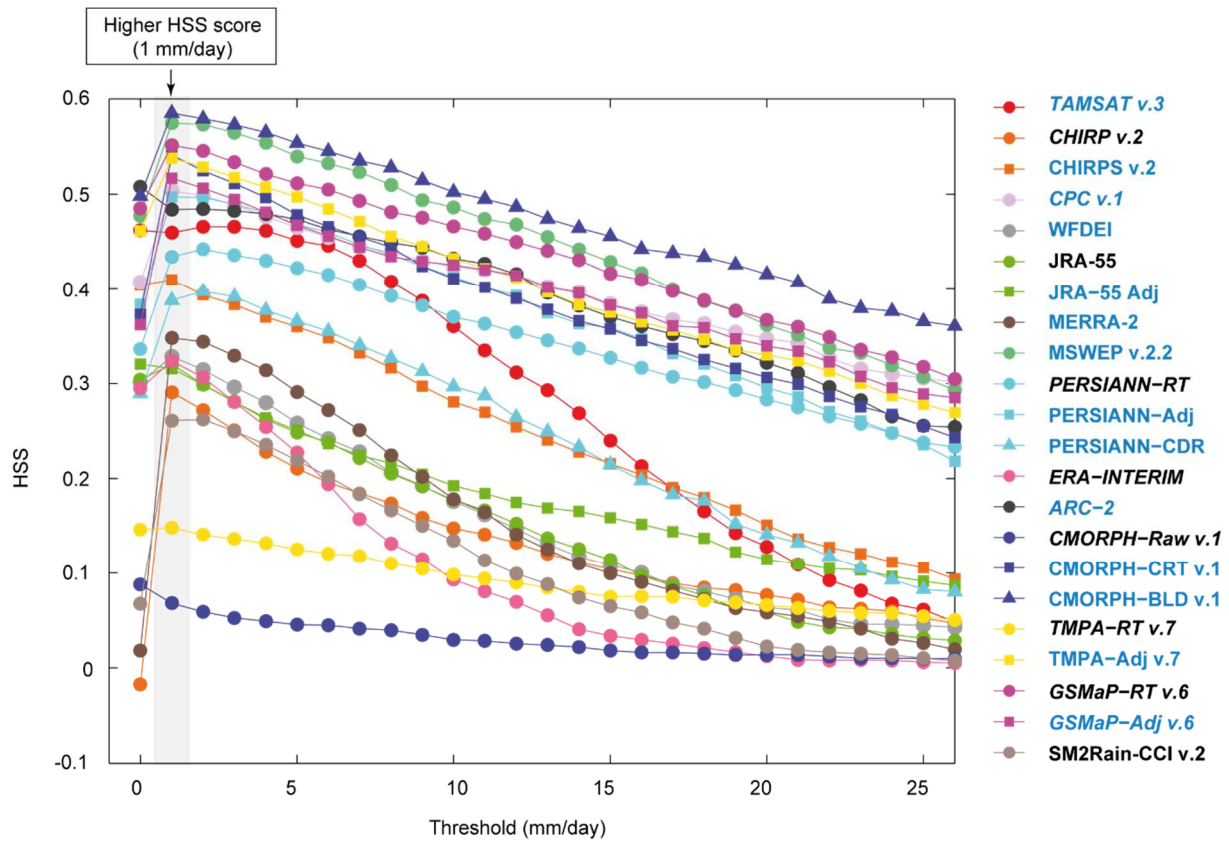


383

384 *Figure 8. P-dataset reliability at the regional scale. The right and left edges of the box represent the 25th and 75th percentile*
 385 *values, respectively. The P-datasets are sorted from the most (top) to the least (bottom) efficient in terms of KGE. SM2Rain-*
 386 *CCI v.2 and GPCP v.7 are at the bottom because their analyses are based on a different number of 0.1° grid-cells, at 79 and*
 387 *183, respectively. Blue and black colours are used to highlight P-datasets using or not using gauge-based information,*
 388 *respectively, and italic font is used for P-datasets available in NRT latency of one to three days. The graphics were inspired*
 389 *by Beck et al. (2019).*

390 Most of the P-datasets presented the highest HSS scores using a threshold value of 1
 391 mm.day⁻¹ (Fig.9). In particular, the HSS values of CHIRP v.2 and MERRA-2 were close to 0 when
 392 considering a 0 mm.day⁻¹ threshold value; the values jumped to 0.3 and 0.36, respectively, when
 393 considering a 1 mm.day⁻¹ threshold value. Actually, the P-datasets detected many precipitation
 394 events with less than 1 mm.day⁻¹ which were not detected by the gauges. This can be explained by
 395 different factors: (1) The gauges are not sensitive enough to such precipitation amounts; (2)
 396 difference in the spatial scale between point (gauge) and average area (P-dataset grid-cell)
 397 measurements; (3) the P-dataset algorithm is deficient. Because these precipitation events are
 398 insignificant (< 1 mm.day⁻¹), they should be considered as no-precipitation events.

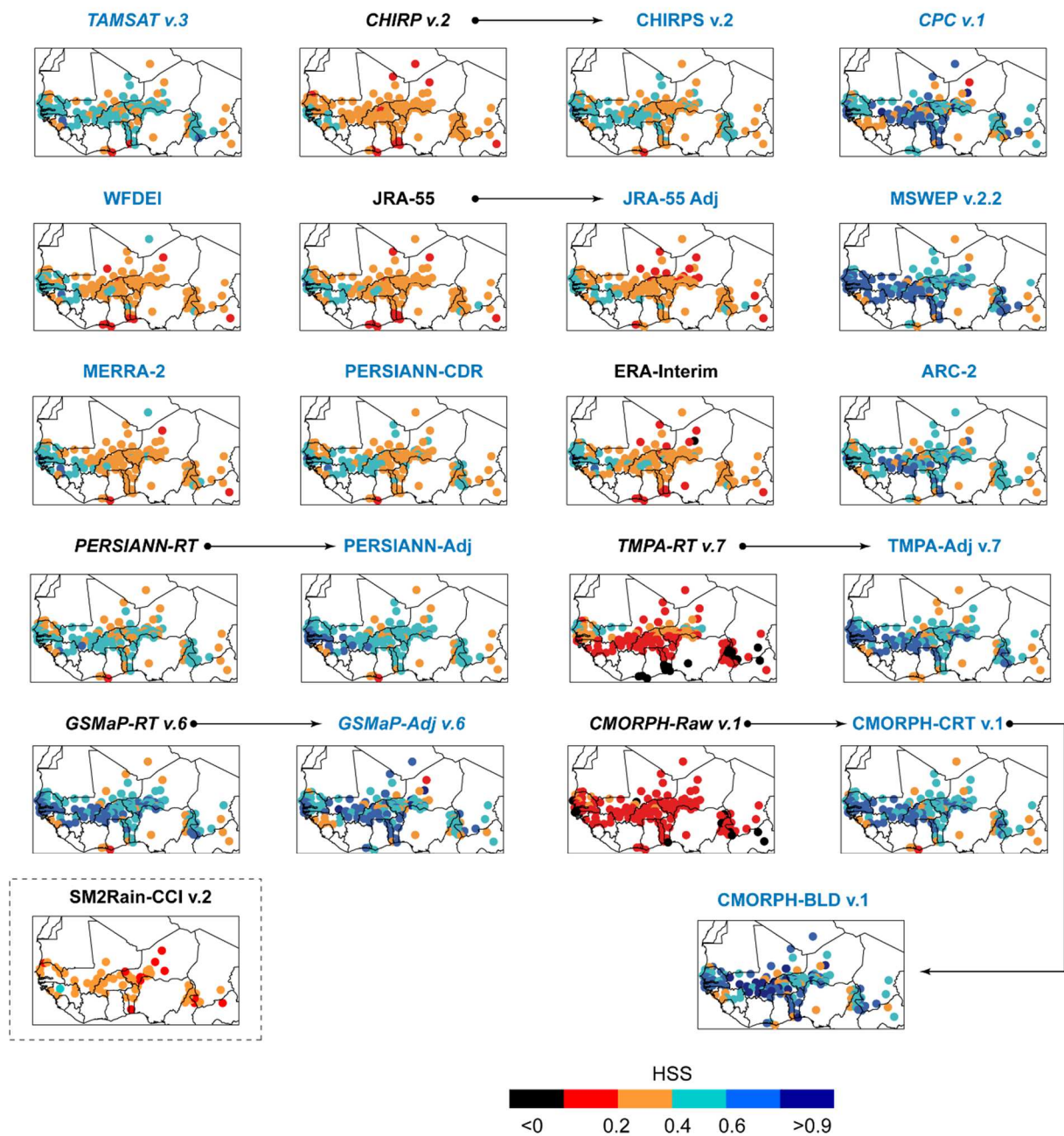
399 The highest HSS score was achieved by CMORPH-BLD v.1 (HSS = 0.58) and MSWEP v.2.2 (HSS
400 = 0.55). The P-dataset ability in reproducing daily precipitation amounts decreased for increasing
401 intensity. Two P-dataset groups measured differently events of more than 15 mm.day⁻¹. The first
402 group (CMORPH-CRT and BLD v.1, GSMaP-RT and Adj v.6, MSWEP v.2.2, PERSIANN-RT and -Adj, ARC-
403 2, and CPC and TMPA-Adj v.7) was much more suited for reproducing high-intensity precipitation
404 events than the second group (CHIRP, CHIRPS, CMORPH-RAW v.1, JRA-55, JRA-55 Adj, PERSIANN-
405 CDR, TAMSAT v.3, TMPA-RT v.7, WFDEI, MERRA-2, ERA-Interim, and SM2Rain CCI v.2). It is worth
406 mentioning that the first group includes (i) P-datasets with gauge-based calibration using daily data
407 and (ii) P-datasets available at the sub-daily time step. The second group includes (i) non-adjusted P-
408 datasets or (ii) those adjusted with monthly gauges-based data, (iii) P-datasets delivered at the daily
409 time step, and (iv) reanalysis P-datasets which generally have the largest discrepancies when
410 compared with other P-datasets (Sun et al., 2018a). Therefore, the gauge-based information used for
411 P-datasets and the delivered time step (daily or sub-daily) considerably influence the P-dataset
412 reliability at the daily time scale. This point is further discussed in section 4 in the Discussion.



413

414 *Figure 9. P-dataset ability in reproducing daily precipitation events of different intensities expressed in the form of HSS. Blue*
 415 *and black colours are used to highlight P-datasets using or not using gauge-based information, respectively, and italic font is*
 416 *used for P-dataset available in NRT latency of one to three days.*

417 Using gauge-based information improved the HSS score over space. For instance, TMPA-RT
 418 v.7 , CMORPH-Raw v.1, CHIRP v.2 and PERSIANN-RT adjusted versions provided much better HSS
 419 scores throughout the region. The adjusted versions of JRA-55, and GSMaP-RT v.6 did not show
 420 significant enhancement. Overall, the first group identified in Fig. 9 (CMORPH-CRT and BLD v.1,
 421 GSMaP-RT and Adj v.6, MSWEP v.2.2, PERSIANN-RT and -Adj, ARC-2, CPC and TMPA-Adj v.7) presents
 422 the highest HSS all over West Africa.



423

424 *Figure 10. Daily P-dataset reliability expressed in the form of HSS considering all days for 2000–2003 period. The HSS was*
 425 *obtained for a threshold value of 1 mm/month. Arrows are used to highlight the potential benefit of using gauge-based*
 426 *information. Blue and black colours are used to highlight P-datasets using or not using gauge-based information,*
 427 *respectively, and italic font is used for P-datasets available in NRT latency of one to three days.*

428

429 4. Discussion

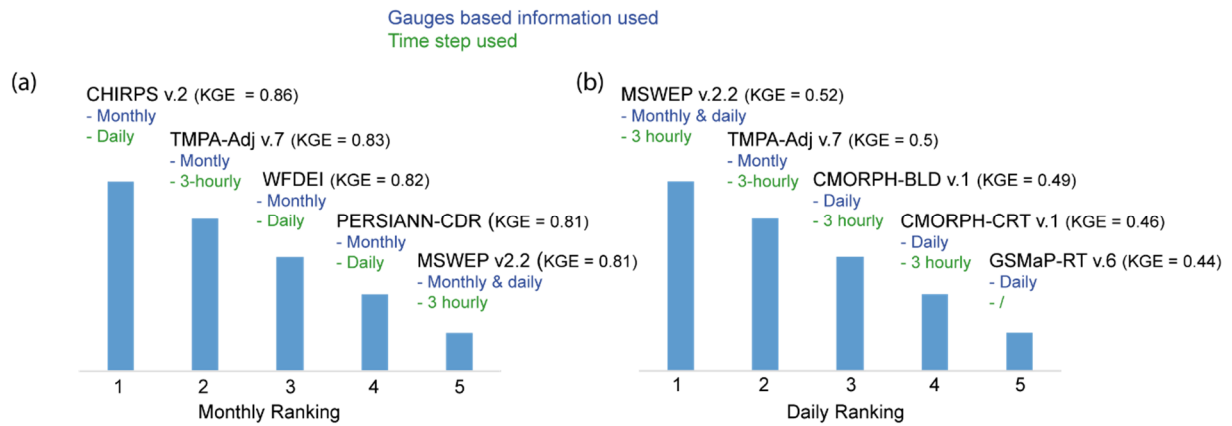
430 4.1. Monthly versus daily P-dataset reliability

431 Interestingly, the P-dataset performance ranking differed at the monthly and daily timescale
432 (Fig. 11). We identified two main factors to explain these discrepancies.

433 The first is related to the gauge-based information time step used to adjust P-dataset
434 estimates. Indeed, the five most efficient P-datasets at the monthly time step, CHIRPS v.2, TMPA-Adj
435 v.7, WFDEI, PERSIANN-CDR, and MSWEP v2.2, were adjusted using monthly gauge-based
436 information, whereas three of the five most efficient P-datasets at the daily time step, MSWEP v.2.2,
437 CMORPH-BLD v.1, and CMORPH-CRT v.1, were adjusted using daily gauge-based information (Fig.
438 11). Additionally, the reliability of the gauge-based information can also influence the P-dataset
439 accuracy. Accordingly, over the Sahel region, the CHPclim monthly dataset reliability was higher than
440 that of GPCC (Funk et al., 2015). Because most of the considered grid-cells used to assess P-dataset
441 reliability are in the Sahel region (Fig. 1), CHIRPS, which uses CHPclim, provides more realistic
442 monthly precipitation estimates, at KGE = 0.86, than WFDEI and PERSIANN-CDR, which uses GPCC
443 and GPCP, respectively (Fig. 3). This demonstrates the importance of maintaining reliable gauge
444 networks to insure accurate P-dataset estimates.

445 The second factor is the P-datasets delivered time step. Some P-datasets are delivered at the
446 daily aggregation level (Table 1), which is based on different time windows than those used for local
447 records. For example, PERSIANN-CDR daily estimates correspond to a given 0 h to 0 h UTC
448 aggregation time period, whereas the gauges used in this study register daily amount from 8 h to 8 h
449 UTC. Such temporal inconsistency can introduce large differences between the P-datasets and the
450 gauge measurements (Ashouri et al., 2015; Satgé et al., 2019). Therefore, only one of the P-datasets,
451 CMORPH-BLD v.1, delivered at the daily time step ranked in the top five most efficient P-datasets. On
452 the contrary, four of the five most efficient P-datasets at the daily time step were delivered at the
453 sub-daily time step (3-hourly) (Table 1 and Fig. 11). The 3-hourly time step enables matching of the
454 computed daily estimates with the local record time windows to ensure consistent comparison
455 between gauges and P-dataset estimates.

456 Our results demonstrate the importance of considering both daily and monthly time steps
 457 when assessing P-dataset reliability because the latter is influenced by the gauge-based adjustment
 458 process and the delivered time step.



459
 460 *Figure 11. P-dataset top-five ranking for the (a) monthly and (b) daily precipitation estimates based on their median KGE*
 461 *value.*

462 Generally, P-datasets using gauge-based information achieved highest KGE scores at both
 463 monthly and daily time step (Figs. 3 and 8), which supports previous results obtained over West
 464 African regions (Casse et al., 2015; Gosset et al., 2013; Poméon et al., 2017) and elsewhere (Beck et
 465 al., 2019; Dinku et al., 2007; Satgé et al., 2017a). However, the use of gauge-based information for P-
 466 dataset adjustment is not always as effective. Indeed, GSMaP-RT v.6 outperformed its adjusted
 467 version GSMaP-Adj v.6 at the daily time step. This result is consistent with previous observation over
 468 the CONUS, (Beck et al., 2019) and illustrates the potential limit P-dataset algorithm to consider the
 469 best of gauge data. GSMaP-RT v.6 is the only P-dataset with no gauge-based information of the top-
 470 five daily ranking. Therefore, GSMaP-Adj v.6 should be highly effective if using the gauge-based
 471 information in the optimal form.

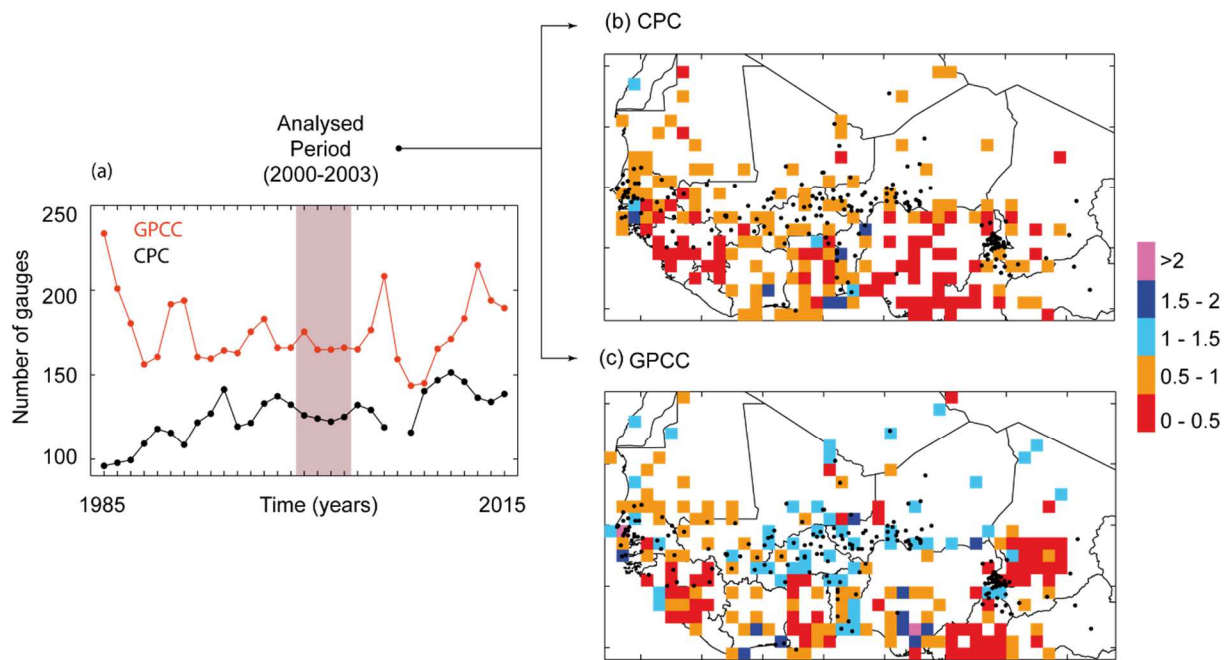
472 4.2. P-dataset reliability in space and time

473 CMORPH-BLD v.1, CMORPH-CRT v.1, GSMaP-Adj v.6, and MERRA-2 presented weaker
 474 performance over the western region in comparison with other P-datasets (Fig. 3). We identified one
 475 factor to explain this spatial inconsistency.

476 Different from other P-datasets which use GPCC or GPCP data, CMORPH-BLD v.1, GSMaP-Adj
477 v.6, and MERRA-2 use CPC data. The gauge number used to retrieve CPC is lower than that used to
478 retrieve GPCC (Fig. 12a). Over the Senegal, Gambia, Guinea-Bissau, and Guinea regions only two CPC
479 grid-cells counted with more than one gauge against seven for GPCC (Fig. 12b and c). As a result,
480 compared with GPCC v.7, CPC v.1 presents the lowest efficiency over the western region (Fig. 4),
481 which propagates into the use of CPC by the P-datasets to adjust their estimates.

482 The available gauge information for retrieving CPC and GPCC datasets also varies with time
483 (Fig. 12a). Therefore, the P-dataset reliability could be better (worse) if considering a period with
484 more (fewer) available gauges for retrieving GPCC or CPC datasets. In this context, TAMSAT v.3 uses
485 consistent gauge-based information in space and time rather than a continuously updated
486 information to avoid adding any space or time discrepancy (Maidment et al., 2017).

487 Actually, P-datasets present space and time inconsistencies which cannot be reported by
488 using single temporal windows (Satgé et al., 2019). The authors assessed P-dataset reliability over
489 three different four years period and one twelve years period across the Lake Titicaca region. Results
490 show that the P-dataset reliability conclusion vary according to the considered period. Therefore,
491 the analysis should be conducted over different temporal windows to adequately evaluate the P-
492 dataset space and time reliability. Such a consideration is challenging over West Africa owing to the
493 scarcity of gauge networks and the important temporal gaps present. To overcome this issue, an
494 alternative method could use satellite-based soil moisture estimates rather than traditional rain
495 gauges measurements as a reference benchmark (Massari et al., 2017).



496

497 *Figure 12. (a) Mean numbers of available gauges used to retrieve GPCCC and CPC for 1985–2015 and their spatial distribution*
 498 *for the analysed period 2000–2003 (b,c). The black points in (b) and (c) represent the centroid of the 0.1° grid-cell considered*
 499 *in this study to assess P-dataset reliability.*

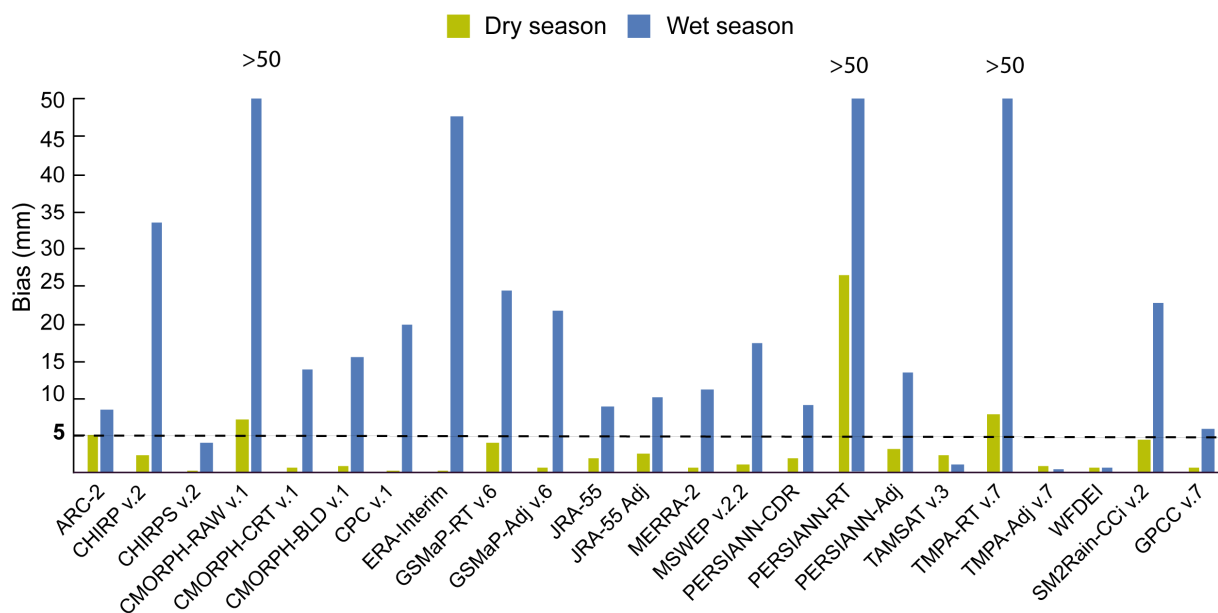
500 It is worth mentioning that GPCCC and CPC share common gauges with the reference network used in
 501 this study as highlighted by many overlapping between both network (Fig. 12 b and c). Similar
 502 observation should be done if considering the others gauges based datasets used for P-dataset
 503 calibration and presented in section 2.2.1. Therefore, the gauges network used for the assessment is
 504 not totally independent of the considered P-datasets and could influence P-dataset reliability
 505 conclusions. The P-dataset reliability conclusion could have been less optimist if only based on
 506 independent gauges network. In this context, future studies should try to consider totally
 507 independent gauges network to provide more consistent feedback on actual P-dataset reliability.
 508 However, information on the shared information between national gauges networks and gauges
 509 based dataset (i.e. CPC and GPCCC) is hard to obtain and compromise this kind of consideration.

510 **4.3. P-datasets sensitivity to seasonal variation**

511 Reanalysis P-datasets, ERA-Interim, MERRA-2, JRA-55 and WFDEI, performed better during the dry
512 than during the wet season (Fig. 3). This agrees with previous results obtained over the CONUS (Beck
513 et al., 2019). The authors explained that reanalysis P-datasets are better adapted to detecting large-
514 scale stratiform systems, which are typical in the dry season, than unpredictable small-scale
515 convective cells, which are typical in the wet season. On the contrary, only satellite-based P-datasets
516 performed better during the wet than the dry season (Beck et al., 2019; Salles et al., 2019; Satgé et
517 al., 2017a). Actually, the irregular sampling of the low earth orbiting satellites and the limited
518 number of overpasses hardly captures short precipitation events which are typical during the dry
519 season (Gebregiorgis and Hossain, 2013; Tian et al., 2009). Therefore, GSMaP-RT v.6 presented a
520 better KGE value during the wet than that during the dry season (Fig. 3). The seasonality sensitivity of
521 the other P-datasets incorporating satellite, reanalysis, or gauge-based information shows a greater
522 contrast because they consider the different inputs.

523 Despite the seasonal variation in KGE value, the P-datasets presented significantly higher
524 coefficient correlation during the dry season (Fig. 3). This difference could be related to the higher
525 monthly precipitation variability during the dry season (Fig. 1) tending to increase the correlation
526 coefficient. Accordingly, all P-datasets presented higher correlation coefficients considering the
527 entire period because the precipitation variability is even more marked than at the seasonal scale. At
528 the contrary, the P-datasets were more biased during the dry season (Fig. 3) except for CPC v.1,
529 GSMaP-Adj v.6, and ERA-Interim. The P-datasets with higher (TAMSAT v.3, PERSIANN-Adj, ARC-2,
530 GSMaP-RT v.6, SM2Rain CCI v.2, JRA-55 Adj, and GPCC v.7) and lower (CPC v.1, GSMaP-Adj v.6, and
531 ERA-Interim) bias values during the dry season presented higher KGE scores during the dry season
532 whereas the P-datasets with close bias values for both wet and dry seasons (CHIRPS v.2, TMPA-Adj
533 v.7, WFDEI, PERSIANN-CDR, MSWEP v2.2, CMORPH-CRT v.1, CHIRP v.2) presented similar KGE values
534 for both seasons. Considering the similar seasonal trend observed for both KGE and bias values, the
535 bias appears to have a dominant influence on the KGE score.

536 Interestingly, if considering the P-dataset bias in millimetres, all P-datasets had systematically
 537 higher bias values during the wet season (Fig. 13). Because lower monthly precipitation occurred
 538 during the dry season, the same volumetric error (millimetres) expressed in ratio (Eq.2) corresponds
 539 to higher bias during the dry in comparison to that during the wet season. For most of the P-datasets,
 540 the reported bias value during the dry season was less than 5 mm.month⁻¹ (Fig. 13), which should
 541 have an insignificant influence on the water budget.

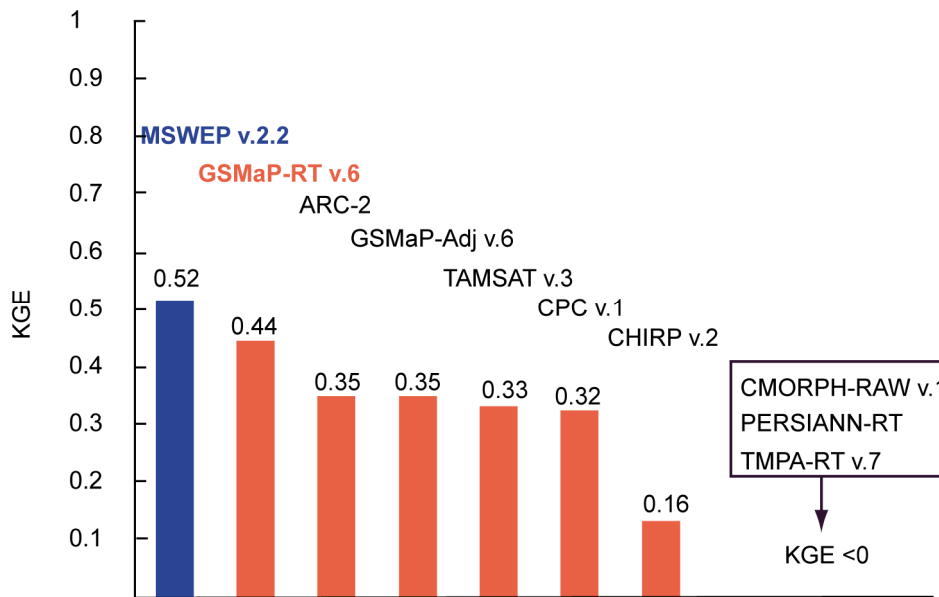


542
 543 *Figure 13: Monthly bias value expressed in millimetres for both dry and wet seasons. The values are expressed in terms of*
 544 *absolute values. To facilitate the analysis, bias values greater than 50 mm are not shown.*

545 Therefore, despite the low KGE value during the dry season, P-datasets still provide valuable
 546 additional information to follow both temporal and volume monthly precipitation dynamics over
 547 West Africa.

548 **4.4. P-dataset time latency**

549 Fig. 14 shows the KGE scores of the NRT P-datasets in comparison with the most accurate P-dataset
 550 at the daily time step.



551

552 *Figure 14. NRT P-dataset reliability at both daily time steps in comparison to the most effective P-datasets, represented in*
 553 *blue.*

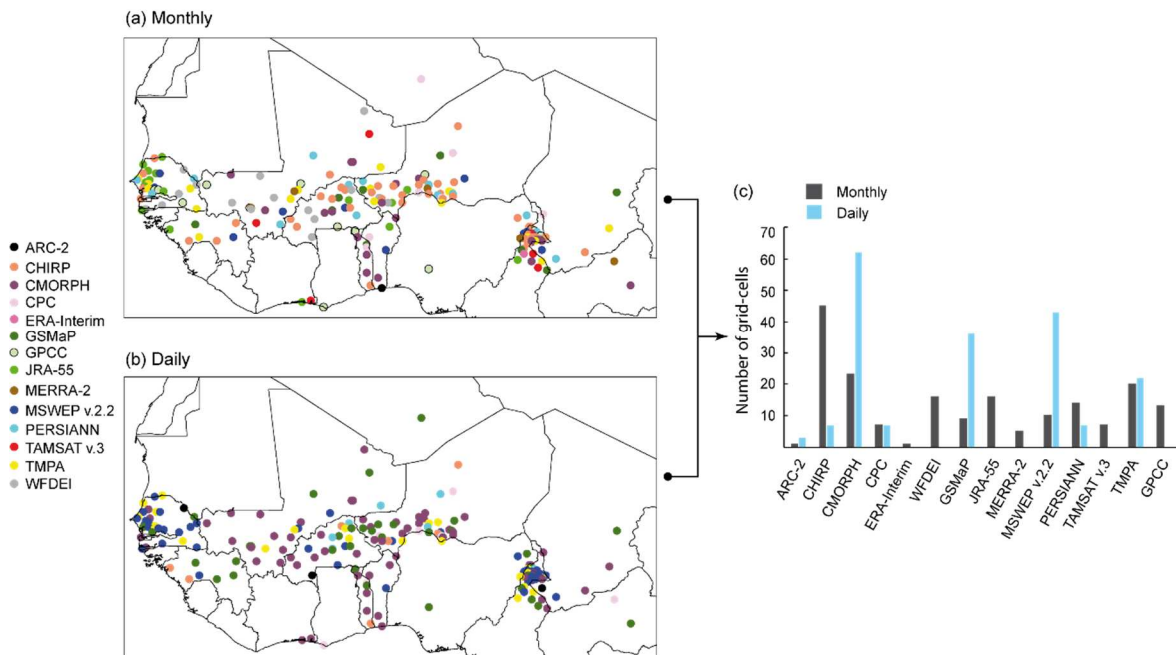
554 At the daily time step, GSMaP-RT v.6 was the most reliable NRT P-dataset. With three days of time
 555 latency, the GSMaP-RT KGE, at 0.44, was close to the most effective P-dataset (MSWEP v2.2) with
 556 KGE = 0.52, which is available with a few months of latency.

557 It is worth mentioning that the low score achieved by the P-datasets at the daily time step is partly
 558 related to the difference between spatially averaged (P-dataset grid-cell) and point (reference
 559 gauges) measurements (Salles et al., 2019; Satgé et al., 2019; Tang et al., 2018). The P-dataset
 560 reliability increased with the number of gauges used to represent the spatially average grid-cell
 561 measurement (Salles et al., 2019; Tang et al., 2018). In this study, most of the considered 0.1° grid-
 562 cells were counted with only one gauge. Therefore, the presented KGE score may underestimate the
 563 actual P-dataset reliability. Testing the sensitivity of streamflow modelling to P-datasets at basin
 564 outlets overcome the influence of scarce and unevenly distributed gauge networks. Indeed,
 565 aggregation of precipitation at the basin scale eliminates the difference in spatial representation
 566 between point (gauge) and areal (P-datasets) measurements because both gauge and P-datasets
 567 represent precipitation at the basin spatial scale. Therefore, the reliability of P-datasets varies
 568 significantly when used to reproduce gauge precipitation estimates or streamflow observations
 569 (Satgé et al. 2019).

570 In this context, NRT P-dataset coverage and latency can fit the needs of an early warning system
571 across sparsely gauged or ungauged regions. Recent studies have successfully used NRT P-datasets to
572 follow flood events in terms of streamflow (Yuan et al., 2019) and flood extent (Belabib et al., 2019)
573 or for landslide occurrence estimations (Brunetti et al., 2018). Future studies should assess NRT P-
574 datasets in the scope of early warning studies to consistently evaluate NRT dataset reliability in this
575 specific context.

576 **4.5. Towards an enhanced P-dataset over West Africa**

577 This study considers an unprecedented sample of 23 P-datasets over the West African region to
578 provide a consistent guideline for potential users. The results suggest that during 2000–2003, CHIRPS
579 v.2 and MSWEP v.2.2 showed the best estimates of monthly and daily precipitation, respectively. The
580 most reliable P-dataset can change at the local scale. As an example, Fig. 15 shows the most suitable
581 P-datasets for representing both monthly and daily precipitation at the grid-cell level. Interestingly,
582 at the daily time step, MSWEP v.2.2 was more consistent for the western region, whereas CMORPH
583 P-datasets provided more accurate estimates over the central and southern regions (Fig. 15). At the
584 monthly time step, even if CHIRP(S) P-datasets are counted with the highest number of grid-cells,
585 large spatial heterogeneity is observed with many grid-cells where WFDEI, JRA-55 Adj, CMORPH, and
586 TMPA outperformed CHIRP(S) (Fig. 15). To take advantage of all available P-datasets, merging all P-
587 datasets to produce an enhanced P-dataset over the region is a good option. Previous studies have
588 reported on the benefit of such an approach to retrieve a more realistic P-dataset over Pakistan
589 (Muhammad et al., 2018; Rahman et al., 2018), Tibet (Ma et al., 2018) and different tropical complex
590 terrain (Bhuiyan et al., 2019). These ensemble precipitation datasets enhance the regional
591 precipitation representation and should be used as guideline over West Africa.



592

593 *Figure 15. Most efficient P-datasets at the grid-cell level. For simplification, the P-datasets were aggregated in main groups:*
 594 *GSMaP = GSMaP-RT + Adj v.6; TMPA = TMPA-RT + TMPA-Adj; JRA-55 = JRA-55 + JRA-55 Adj; PERSIANN = PERSIANN-RT +*
 595 *PERSIANN-Adj + PERSIANN-CDR.*

596 5. Conclusions

597 The present study evaluates the accuracy of 23 gridded P-datasets over the West African region at
 598 both monthly and daily time step for the 2000-2003 period. Despite the limited coverage and scarcity
 599 of the ground reference points, some consistent features emerged from the analysis:

- 600 • The P-dataset performance ranking differs at the monthly and daily timescale. P-datasets
 601 using sub-daily (monthly) gauge information perform better at the daily (monthly) time step.
 602 Additionally, for the P-datasets released at the daily time step, the temporal mismatch
 603 between gauge and satellite reporting times decrease their reliability at the daily time step.
 604 In this line, MSWEP v.2.2 and CHIRPS v.2 provide the most reliable daily and monthly
 605 precipitation estimates, respectively whereas TMPA-Adj v.7 performance is very good for
 606 both daily and monthly estimates.

- 607 • The only satellite based P-datasets (CMORPH-RT v.1, TMPA-RT v.7, PERSIANN-RT, GSMaP v.6-
608 RT) performance is very low at both monthly and daily time scale. Their reliability drastically
609 increase for their adjusted versions (CMORPH-CRT and BLD v.1, TMPA-Adj v.7, PERSIANN-
610 Adj) excepted for GSMaP v.6 at the daily time step.
- 611 • All the considered reanalysis P-datasets (WFDEI, JRA-55, JRA-55 Adj, ERA-Interim) are
612 unreliable at the daily time step. The use of monthly GPCC P-dataset to adjust their estimates
613 considerably increase their reliability at the monthly time step (WFDEI, JRA-55 Adj).
- 614 • The two African P-datasets (TAMSAT v.3 and ARC-2) present an overall lower performance in
615 comparison to the almost global scale P-datasets at both daily and monthly time-step.
616 Despite good performance in some parts of the region, SM2Rain-CCI v.2 still suffers too many
617 gaps in space and time across West African.
- 618 • All P-datasets present spatial discrepancies in their statistical score suggesting the use of a
619 spatial P-datasets' merging approach to take advantage from all available P-datasets across
620 West Africa.

621 It should be reminded that most of the considered 0.1° grid-cells count with only one gauge to
622 represent the observed precipitation. Because of spatial inconsistency between point (gauges) and
623 spatially average (P-datasets) measurement, different conclusion regarding the P-datasets reliability,
624 could have been drawn if more gauges had been available per grid-cells or if using P-datasets as
625 forcing data for hydrological modelling. Additionally, the study is based on a single four years
626 temporal window. However, P-dataset reliability vary in time and the results could have been
627 different if considering another four years temporal window or a larger one. Therefore, this study
628 aims more at compare the P-dataset reliability between them rather than to provide definitive
629 conclusion on their respective accuracy.

630 **References**

631 Abiodun, B. J., Adeyewa, Z. D. and Ajayi, V. O.: Modeling the impacts of reforestation on future

632 climate in West Africa, , 77–96, doi:10.1007/s00704-012-0614-1, 2012.

633 Adler, R. F., Huffman, G. J., Chang, A., Ferraro, F., Xie, P.-P., Janowiak, J., Rudolf, B., Schneider, U.,
634 Curtis, S., Bolvin, D., Gruber, A., Susskind, J., Arkin, P. and Nelkin, E.: The Version-2 Global
635 Precipitation Climatology Project (GPCP) Monthly Precipitation Analysis (1979 – Present), J.
636 Hydrometeorol., (January 1997), 1147–1167, 2003.

637 Adler, R. F., Gu, G. and Huffman, G. J.: Estimating Climatological Bias Errors for the Global
638 Precipitation Climatology Project (GPCP), J. Appl. Meteorol. Climatol., (2008), 84–99,
639 doi:10.1175/JAMC-D-11-052.1, 2012.

640 Agutu, N. O., Awange, J. L., Zerihun, A., Ndehedehe, C. E., Kuhn, M. and Fukuda, Y.: Assessing multi-
641 satellite remote sensing, reanalysis, and land surface models' products in characterizing agricultural
642 drought in East Africa, Remote Sens. Environ., 194, 287–302, doi:10.1016/j.rse.2017.03.041, 2017.

643 Akinsanola, A. A., Ogunjobi, K. O., Ajayi, V. O., Adefisan, E. A., Omotosho, J. A. and Sanogo, S.:
644 Comparison of five gridded precipitation products at climatological scales over West Africa
645 Comparison of five gridded precipitation products at climatological scales over West Africa,
646 Meteorol. Atmos. Phys., (February 2018), doi:10.1007/s00703-016-0493-6, 2016.

647 Anjum, M. N., Ding, Y., Shangguan, D., Tahir, A. A., Iqbal, M. and Adnan, M.: Comparison of two
648 successive versions 6 and 7 of TMPA satellite precipitation products with rain gauge data over Swat
649 Watershed, Hindukush Mountains, Pakistan, Atmos. Sci. Lett., 17(4), 270–279, doi:10.1002/asl.654,
650 2016.

651 Arvor, D., Funatsu, B., Michot, V. and Dubreuil, V.: Monitoring Rainfall Patterns in the Southern
652 Amazon with PERSIANN-CDR Data: Long-Term Characteristics and Trends, Remote Sens., 9(9), 889,
653 doi:10.3390/rs9090889, 2017.

654 Ashouri, H., Hsu, K. L., Sorooshian, S., Braithwaite, D. K., Knapp, K. R., Cecil, L. D., Nelson, B. R. and
655 Prat, O. P.: PERSIANN-CDR: Daily precipitation climate data record from multisatellite observations

656 for hydrological and climate studies, *Bull. Am. Meteorol. Soc.*, 96(1), 69–83, doi:10.1175/BAMS-D-13-
657 00068.1, 2015.

658 Awange, J. L., Ferreira, V. G., Forootan, E., Andam-akorful, S. A. and Agutu, N. O.: Uncertainties in
659 remotely sensed precipitation, , 323(April 2015), 303–323, doi:10.1002/joc.4346, 2016.

660 Beck, H. E., Wood, E. F., Pan, M., Fisher, C. K., Miralles, D. G., Van Dijk, A. I. J. M., McVicar, T. R. and
661 Adler, R. F.: MSWEP V2 GLOBAL 3-HOURLY 0.1° PRECIPITATION Methodology and Quantitative
662 Assessment, *Bull. Am. Meteorol. Soc.*, (March), 473–500, doi:10.1175/BAMS-D-17-0138.1, 2018.

663 Beck, H. E., Pan, M., Roy, T., Weedon, G. P., Pappenberger, F., Dijk, A. I. J. M. Van, Huffman, G. J.,
664 Adler, R. F. and Wood, E. F.: Daily evaluation of 26 precipitation datasets using Stage-IV gauge-radar
665 data for the CONUS, , 207–224, 2019.

666 Becker, A., Finger, P., Rudolf, B., Schamm, K., Schneider, U., Ziese, M., Precipitation, G., Centre, C. and
667 Wetterdienst, D.: A description of the global land-surface precipitation data products of the Global
668 Precipitation Climatology Centre with sample applications including centennial (trend) analysis from
669 1901–present, , 71–99, doi:10.5194/essd-5-71-2013, 2013.

670 Belabib, N., Zhao, F., Brocca, L., Huang, Y. and Tan, Y.: Near-Real-Time Flood Forecasting Based on
671 Satellite Precipitation Products, *Remote Sens.*, 11, doi:10.3390/rs11030252, 2019.

672 Bhuiyan, M. A. E., Nikolopoulos, E. I. and Anagnostou, E. N.: Machine Learning-based Blending of
673 Satellite and Reanalysis Precipitation Datasets : A Multi-regional Tropical Complex Terrain Evaluation,
674 *J. hydrometeorol*, 6806(860), 1–42, doi:10.1175/JHM-D-19-0073.1., 2019.

675 Brunetti, M. T., Melillo, M., Peruccacci, S., Ciabatta, L. and Brocca, L.: Remote Sensing of Environment
676 How far are we from the use of satellite rainfall products in landslide forecasting ?, *Remote Sens.*
677 *Environ.*, 210, 65–75, doi:10.1016/j.rse.2018.03.016, 2018.

678 Carvalho, L. M. V., Jones, C., Posadas, A. N. D., Quiroz, R., Bookhagen, B. and Liebman, B.:
679 Precipitation Characteristics of the South American Monsoon System Derived from Multiple

680 Datasets, *J. Clim.*, 25, 4600–4620, doi:10.1175/JCLI-D-11-00335.1, 2012.

681 Casse, C., Gosset, M., Peugeot, C., Pedinotti, V., Boone, a., Tanimoun, B. a. and Decharme, B.:
682 Potential of satellite rainfall products to predict Niger River flood events in Niamey, *Atmos. Res.*,
683 doi:10.1016/j.atmosres.2015.01.010, 2015.

684 Chen, M., Shi, W., Xie, P., Silva, V. B. S., Kousky, V. E., Higgins, R. W. and Janowiak, J. E.: Assessing
685 objective techniques for gauge-based analyses of global daily precipitation, *J. Geophys. Res.*, 113, 1–
686 13, doi:10.1029/2007JD009132, 2008.

687 Collischonn, B., Collischonn, W. and Tucci, C. E. M.: Daily hydrological modeling in the Amazon basin
688 using TRMM rainfall estimates, *J. Hydrol.*, 360(1–4), 207–216, doi:10.1016/j.jhydrol.2008.07.032,
689 2008.

690 Cosgrove, W. J. and Risberman, F. R., Eds.: world water vision, Earthscan Publications Ltd, London.,
691 2000.

692 Dembélé, M. and Zwart, S. J.: Evaluation and comparison of satellite-based rainfall products in
693 Burkina Faso , West Africa, *Int. J. Remote Sens.*, 37(17), 3995–4014,
694 doi:10.1080/01431161.2016.1207258, 2016.

695 Dinku, T., Ceccato, P., Grover-Kopec, E., Lemma, M., Connor, S. J. and Ropelewski, C. F.: Validation of
696 satellite rainfall products over East Africa’s complex topography, *Int. J. Remote Sens.*, 28(7), 1503–
697 1526, doi:10.1080/01431160600954688, 2007.

698 Dorigo, W. A., Gruber, A., De Jeu, R. A. M., Wagner, W., Stacke, T., Loew, A., Albergel, C., Brocca, L.,
699 Chung, D., Parinussa, R. M. and Kidd, R.: Evaluation of the ESA CCI soil moisture product using
700 ground-based observations, *Remote Sens. Environ.*, 162, 380–395, doi:10.1016/j.rse.2014.07.023,
701 2015.

702 Doumounia, A., Gosset, M., Cazenave, F., Kacou, M. and Zougmore, F.: Rainfall monitoring based on
703 microwave links from cellular telecommunication networks: First results from a West African test

704 bed, *Geophys. Res. Lett.*, 41(16), 6015–6021, doi:10.1002/2014GL060724, 2014.

705 Ferraro, R. R., Smith, E. A., Berg, W. and Huffman, G. J.: A Screening Methodology for Passive
706 Microwave Precipitation Retrieval Algorithms, *J. Atmos. Sci.*, 55(9), 1583–1600, doi:10.1175/1520-
707 0469(1998)055<1583:ASMFPM>2.0.CO;2, 1998.

708 Fick, S. E. and Hijmans, R. J.: WorldClim 2 : new 1-km spatial resolution climate surfaces for global
709 land areas, *Int. J. Climatol.*, 4315(May), 4302–4315, doi:10.1002/joc.5086, 2017.

710 Fischer, E. M. and Knutti, R.: Anthropogenic contribution to global occurrence of heavy-precipitation
711 and high-temperature extremes, *Nat. Clim. Chang.*, 5(April), doi:10.1038/NCLIMATE2617, 2015.

712 Funk, C., Verdin, A., Michaelsen, J., Peterson, P., Pedreros, P. and Husak, G.: A global satellite-assisted
713 precipitation climatology, *Earth Syst. Sci. Data*, 7, 275–287, doi:10.5194/essd-7-275-2015, 2015.

714 Gao, Z., Long, D., Tang, G., Zeng, C., Huang, J. and Hong, Y.: Assessing the potential of satellite-based
715 precipitation estimates for flood frequency analysis in ungauged or poorly gauged tributaries of
716 China ' s Yangtze River basin, *J. Hydrol.*, 550, 478–496, doi:10.1016/j.jhydrol.2017.05.025, 2017.

717 Gebregiorgis, A. S. and Hossain, F.: Understanding the Dependence of Satellite Rainfall Uncertainty
718 on Topography and Climate for Hydrologic Model Simulation, *IEEE Trans. Geosci. Remote Sens.*,
719 51(1), 704–718, doi:10.1109/TGRS.2012.2196282, 2013.

720 Giorgi, F., Coppola, E. and Raffaele, F.: Threatening levels of cumulative stress due to hydroclimatic
721 extremes in the 21st century, *npj Clim. Atmos. Sci.*, (March), doi:10.1038/s41612-018-0028-6, 2018.

722 Gosset, M., Viarre, J., Quantin, G. and Alcoba, M.: Evaluation of several rainfall products used for
723 hydrological applications over West Africa using two high-resolution gauge networks, *Q. J. R.*
724 *Meteorol. Soc.*, 139(673), 923–940, doi:10.1002/qj.2130, 2013.

725 Guo, H., Bao, A., Liu, T., Ndayisaba, F., He, D., Kurban, A. and Maeyer, P. De: Meteorological Drought
726 Analysis in the Lower Mekong Basin Using Satellite-Based Long-Term CHIRPS Product, *Sustainability*,

727 (9), doi:10.3390/su9060901, 2017.

728 Hussain, Y., Satgé, F., Hussain, M. B., Martinez-Caravajal, H., Bonnet, M.-P., Cardenas-Soto, M., Llacer
729 Roig, H. and Akhter, G.: Performance of CMORPH, TMPA and PERSIANN rainfall datasets over plain,
730 mountainous and glacial regions of Pakistan, *Theor. Appl. Climatol.*, doi:10.1007/s00704-016-2027-z,
731 2017.

732 Lebel, T., Taupin, J. D. and D'Amato, N.: Rainfall monitoring during HAPEX-Sahel. 1. General rainfall
733 conditions and climatology, *J. Hydrol.*, 189, 74–96, 1997.

734 Levizzani, V., Amorati, R. and Meneguzzo, F.: A review of satellite-based rainfall estimation methods.,
735 2002.

736 Li, J. and D.Heap, A.: Spatial Interpolation Methods: A Review for Environmental Scientists. [online]
737 Available from: http://www.ga.gov.au/corporate_data/68229/Rec2008_023.pdf (Accessed 4
738 November 2014), 2008.

739 Ma, Y., Yang, Y., Han, Z., Tang, G., Maguire, L. and Chu, Z.: Comprehensive evaluation of Ensemble
740 Multi-Satellite Precipitation Dataset using the Dynamic Bayesian Model Averaging scheme over the
741 Tibetan plateau, *J. Hydrol.*, 556, 634–644, doi:10.1016/j.jhydrol.2017.11.050, 2018.

742 Maggioni, V. and Massari, C.: On the performance of satellite precipitation products in riverine flood
743 modeling: A review, *J. Hydrol.*, 558, 214–224, doi:10.1016/j.jhydrol.2018.01.039, 2018.

744 Maggioni, V., Meyers, P. C. and Robinson, M. D.: A Review of Merged High-Resolution Satellite
745 Precipitation Product Accuracy during the Tropical Rainfall Measuring Mission (TRMM) Era, *J.*
746 *Hydrometeorol.*, 17(4), 1101–1117, doi:10.1175/JHM-D-15-0190.1, 2016.

747 Maidment, R. I., Grimes, D., Allan, R. P., Tarnavsky, E., Stringer, M., Hewison, T., Roebeling, R. and
748 Black, E.: The 30 year TAMSAT African Rainfall Climatology And Time series (TARCAT) data set, *J.*
749 *Geophys. Res. Atmos.*, 10619–10644, doi:10.1002/2014JD021927.Received, 2014.

750 Maidment, R. I., Grimes, D., Black, E., Tarnavsky, E., Young, M., Greatrex, H., Allan, R. P., Stein, T.,
751 Nkonde, E., Senkunda, S., Misael, E. and Alcántara, U.: Data Descriptor : A new , long-term daily
752 satellite-based rainfall dataset for operational monitoring in Africa, *Nat. Publ. Gr.*, 4, 1–19,
753 doi:10.1038/sdata.2017.63, 2017.

754 Massari, C., Crow, W. and Brocca, L.: An assessment of the accuracy of global rainfall estimates
755 without ground-based observations, *Hydrol. Earth Syst. Sci. Discuss.*, (April), 1–24, doi:10.5194/hess-
756 2017-163, 2017.

757 Messer, H., Zinevich, A. and Alpert, P.: Environmental monitoring by wireless communication
758 networks, *Science (80-.)*, 312(5774), 713, doi:10.1126/science.1120034, 2006.

759 Muhammad, W., Yang, H., Lei, H., Muhammad, A. and Yang, D.: Improving the regional applicability
760 of satellite precipitation products by ensemble algorithm, *Remote Sens.*, 10(4), 1–19,
761 doi:10.3390/rs10040577, 2018.

762 Nikolopoulos, E. I., Anagnostou, A. N. and Borga, M.: Using High-Resolution Satellite Rainfall Products
763 to Simulate a Major Flash Flood Event in Northern Italy, *J. Hydrometeorol.*, 14, 171–185,
764 doi:10.1175/JHM-D-12-09.1, 2013.

765 Novella, N. S. and Thiaw, W. M.: African Rainfall Climatology Version 2 for Famine Early Warning
766 Systems, *J. Appl. Meteorol. Climatol.*, 52(1996), 588–606, doi:10.1175/JAMC-D-11-0238.1, 2012.

767 Overeem, A., Leijnse, H. and Uijlenhoet, R.: Measuring urban rainfall using microwave links from
768 commercial cellular communication networks, *Water Resour. Res.*, 47(12), 1–16,
769 doi:10.1029/2010WR010350, 2011.

770 De Paiva, R. C. D., Buarque, D. C., Collischonn, W., Bonnet, M. P., Frappart, F., Calmant, S. and
771 Bulhões Mendes, C. A.: Large-scale hydrologic and hydrodynamic modeling of the Amazon River
772 basin, *Water Resour. Res.*, 49(3), 1226–1243, doi:10.1002/wrcr.20067, 2013.

773 Poméon, T., Jackisch, D. and Dieckrüger, B.: *Journal of Hydrology, J. Hydrol.*, 547, 222–235,

774 doi:10.1016/j.jhydrol.2017.01.055, 2017.

775 Prakash, S., Sathiyamoorthy, V., Mahesh, C. and Gairola, R. M.: An evaluation of high-resolution
776 multisatellite rainfall products over the Indian monsoon region, *Int. J. Remote Sens.*, 35(9), 3018–
777 3035, doi:10.1080/01431161.2014.894661, 2014a.

778 Prakash, S., Mitra, A. K. and Momin, I. M.: Comparison of TMPA-3B42 Versions 6 and 7 Precipitation
779 Products with Gauge-Based Data over India for the Southwest Monsoon Period, , 346–362,
780 doi:10.1175/JHM-D-14-0024.1, 2014b.

781 Rahman, K. U., Shang, S. and Shahid, M.: Developing an Ensemble Precipitation Algorithm from
782 Satellite Products and Its Topographical and Seasonal Evaluations Over Pakistan, *Remote Sens.*,
783 doi:10.3390/rs10111835, 2018.

784 Rahmawati, N. and Lubczynski, M. W.: Validation of satellite daily rainfall estimates in complex
785 terrain of Bali Island, Indonesia, *Theor. Appl. Climatol.*, 1–20, doi:10.1007/s00704-017-2290-7, 2017.

786 Ramarohetra, J., Sultan, B., Baron, C., Gaiser, T. and Gosset, M.: Agricultural and Forest Meteorology
787 How satellite rainfall estimate errors may impact rainfed cereal yield simulation in West Africa, *Agric.*
788 *For. Meteorol.*, 180, 118–131, doi:10.1016/j.agrformet.2013.05.010, 2013.

789 Ringard, J., Becker, M., Seyler, F. and Linguet, L.: Temporal and spatial assessment of four satellite
790 rainfall estimates over French Guiana and north Brazil, *Remote Sens.*, 7(12), 16441–16459,
791 doi:10.3390/rs71215831, 2015.

792 Saeed, F., Bethke, I., Fischer, E., Legutke, S., Shiogama, H., Stone, D. A. and Schleussner, C.-P.: Robust
793 changes in tropical rainy season length at OPEN ACCESS Robust changes in tropical rainy season
794 length at 1 . 5 ° C, *Environ. Res. Lett.*, 13, doi:https://doi.org/10.1088/1748-9326/aab797, 2018.

795 Salles, L., Satgé, F., Roig, H., Almeida, T., Olivetti, D. and Ferreira, W.: Seasonal Effect on Spatial and
796 Temporal Consistency of the New GPM-Based IMERG-v5 and GSMaP-v7 Satellite Precipitation
797 Estimates in Brazil’s Central Plateau Region, *Water*, 11, doi:10.3390/w11040668, 2019.

798 Satgé, F., Bonnet, M.-P., Gosset, M., Molina, J., Hernan Yuque Lima, W., Pillco Zolá, R., Timouk, F. and
799 Garnier, J.: Assessment of satellite rainfall products over the Andean plateau, *Atmos. Res.*, 167, 1–14,
800 doi:10.1016/j.atmosres.2015.07.012, 2016.

801 Satgé, F., Xavier, A., Zolá, R., Hussain, Y., Timouk, F., Garnier, J. and Bonnet, M.-P.: Comparative
802 Assessments of the Latest GPM Mission’s Spatially Enhanced Satellite Rainfall Products over the Main
803 Bolivian Watersheds, *Remote Sens.*, 9(4), 369, doi:10.3390/rs9040369, 2017a.

804 Satgé, F., Espinoza, R., Zolá, R., Roig, H., Timouk, F., Molina, J., Garnier, J., Calmant, S., Seyler, F. and
805 Bonnet, M.-P.: Role of Climate Variability and Human Activity on Poopó Lake Droughts between 1990
806 and 2015 Assessed Using Remote Sensing Data, *Remote Sens.*, 9(3), 218, doi:10.3390/rs9030218,
807 2017b.

808 Satgé, F., Ruelland, D., Bonnet, M., Molina, J., Pillco, R., Hydrosciences, U. M. R., Bataillon, P. E.,
809 Cedex, M., Hydrosciences, U. M. R., Bataillon, P. E. and Cedex, M.: Consistency of satellite-based
810 precipitation products in space and over time compared with gauge observations and snow-
811 hydrological modelling in the Lake Titicaca region, *Hydrol. Earth Syst. Sci.*, 23, 595–619,
812 doi:https://doi.org/10.5194/hess-23-595-2019, 2019.

813 Schneider, U., Becker, A., Finger, P., Meyer-christoffer, A., Ziese, M. and Rudolf, B.: GPCCC ’ s new land
814 surface precipitation climatology based on quality-controlled in situ data and its role in quantifying
815 the global water cycle, , 15–40, doi:10.1007/s00704-013-0860-x, 2014.

816 Su, J., Lü, H., Wang, J., Sadeghi, A. M. and Zhu, Y.: Evaluating the applicability of four latest satellite-
817 gauge combined precipitation estimates for extreme precipitation and streamflow predictions over
818 the upper yellow river basins in China, *Remote Sens.*, 9(11), 1–19, doi:10.3390/rs9111176, 2017.

819 Sultan, B., Roudier, P., Quiron, P., Alhassane, A., Muller, B., Dingkuhn, M., Ciais, P., Guimberteau, M.,
820 Traore, S. and Baron, C.: Assessing climate change impacts on sorghum and millet yields in the
821 Sudanian and Sahelian savannas of West Africa, *Environmental Res. Lett.*, 8, doi:10.1088/1748-

822 9326/8/1/014040, 2013.

823 Sun, Q., Miao, C., Duan, Q. and Kong, D.: Would the ‘ real ’ observed dataset stand up ? A critical
824 examination of eight observed gridded climate datasets for China, *Environ. Res. Lett.*, 9,
825 doi:10.1088/1748-9326/9/1/015001, 2015.

826 Sun, Q., Miao, C., Duan, Q., Ashouri, H., Sorroschian, S. and Hsu, K.-L.: A review of global precipitation
827 data sets: data, sources, estimation, and intercomparisons, *Rev. Geophys.*, 56, 79–107,
828 doi:10.1002/2017RG000574, 2018a.

829 Sun, W., Ma, J. and Yang, G.: Statistical and Hydrological Evaluations of Multi-Satellite Precipitation
830 Products over Fujiang River Basin in Humid Southeast China, *Remote Sens.*, 10,
831 doi:10.3390/rs10121898, 2018b.

832 Tang, G., Ma, Y., Long, D., Zhong, L. and Hong, Y.: Evaluation of GPM Day-1 IMERG and TMPA
833 Version-7 legacy products over Mainland China at multiple spatiotemporal scales, *J. Hydrol.*, 533,
834 152–167, doi:10.1016/j.jhydrol.2015.12.008, 2016.

835 Tang, G., Behrangi, A., Long, D., Li, C. and Hong, Y.: Accounting for spatiotemporal errors of gauges: A
836 critical step to evaluate gridded precipitation products, *J. Hydrol.*, 559, 294–306,
837 doi:10.1016/j.jhydrol.2018.02.057, 2018.

838 Thaler, S., Brocca, L., Ciabatta, L., Eitzinger, J., Hahn, S. and Wagner, W.: Effects of Different Spatial
839 Precipitation Input Data on Crop Model Outputs under a Central European Climate, *Atmosphere*
840 (Basel), 9, doi:10.3390/atmos9080290, 2018.

841 Thiemig, V., Rojas, R., Zambrano-Bigiarini, M., Levizzani, V. and De roo, A.: Validation of Satellite-
842 Based Precipitation Products over Sparsely Gauged African River Basins, *J. Hydrometeorol.*, 13(6),
843 1760–1783, doi:10.1175/JHM-D-12-032.1, 2012.

844 Tian, Y., Peters-Lidard, C. D., Eylander, J. B., Joyce, R. J., Huffman, G. J., Adler, R. F., Hsu, K.-L., Turk, F.
845 J., Garcia, M. and Zeng, J.: Component analysis of errors in satellite-based precipitation estimates, *J.*

846 Geophys. Res., 114(D24), D24101, doi:10.1029/2009JD011949, 2009.

847 Toté, C., Patricio, D., Boogaard, H., Wijngaart, R. Van Der, Tarnavsky, E. and Funk, C.: Evaluation of
848 Satellite Rainfall Estimates for Drought and Flood Monitoring in Mozambique, *Remote Sens.*, 7,
849 1758–1776, doi:10.3390/rs70201758, 2015.

850 Wit, A. De, Baruth, B., Boogaard, H., Diepen, K. Van, van Kraalingen, D., Micale, F., Roller, J. te, Supot,
851 I. and Wijngaart, R. van den: Using ERA-INTERIM for regional crop yield forecasting in Europe, *Clim.*
852 *Res.*, 44(June 2014), 41–53, doi:10.3354/cr00872, 2010.

853 Xie, P., Yatagai, A., Chen, M., Hayasaka, T., Fukushima, Y., Liu, C. and Yang, S.: A Gauge-Based Analysis
854 of Daily Precipitation over East Asia, *J. Hydrometeorol.*, 607–626, doi:10.1175/JHM583.1, 2007.

855 Yuan, F., Zhang, L., Min, K., Soe, W., Ren, L. and Zhao, C.: Applications of TRMM- and GPM-Era
856 Multiple- Satellite Precipitation Products for Flood Simulations at Sub-Daily Scales in a Sparsely
857 Gauged Watershed in Myanmar, *Remote Sens.*, doi:10.3390/rs11020140, 2019.

858 Zambrano-Bigiarini, M., Nauditt, A., Birkel, C., Verbist, K. and Ribbe, L.: Temporal and spatial
859 evaluation of satellite-based rainfall estimates across the complex topographical and climatic
860 gradients of Chile, *Hydrol. Earth Syst. Sci.*, 21(2), 1295–1320, doi:10.5194/hess-21-1295-2017, 2017.

861 Zeng, Q., Wang, Y., Chen, L., Wang, Z., Zhu, H. and Li, B.: Inter-comparison and evaluation of remote
862 sensing precipitation products over China from 2005 to 2013, *Remote Sens.*, 10(2),
863 doi:10.3390/rs10020168, 2018.

864 Zhang, Y., Li, Y., Ji, X., Luo, X. and Li, X.: Evaluation and Hydrologic Validation of Three Satellite-Based
865 Precipitation Products in the Upper Catchment of the Red River Basin , China, *Remote Sens.*, 10, 1–
866 22, doi:10.3390/rs10121881, 2018.

867 Zinevich, A., Alpert, P. and Messer, H.: Estimation of rainfall fields using commercial microwave
868 communication networks of variable density, *Adv. Water Resour.*, 31(11), 1470–1480,
869 doi:10.1016/j.advwatres.2008.03.003, 2008.